Dissecting *Trypanosoma brucei* RRP44 function in the maturation of segmented ribosomal RNA using a regulated genetic complementation system

Eloise Pavão Guerra-Slompo[1], Giovanna Cesaro[1,2], Beatriz Gomes Guimarães [ID][1,2] **and Nilson Ivo Tonin Zanchin** [ID][1,*]

[1]Carlos Chagas Institute, Oswaldo Cruz Foundation, FIOCRUZ, R. Prof. Algacyr Munhoz Mader 3775, 81350-010, Curitiba-PR, Brazil and [2]Biochemistry Postgraduate Program, Federal University of Paraná, Curitiba-PR, Brazil

ABSTRACT

***Trypanosoma brucei* belongs to a group of protozoans presenting fragmented large subunit rRNA. Its LSU rRNA equivalent to the 25S/28S rRNA of other eukaryotes is split into six fragments, requiring additional processing for removal of the extra spacer sequences. We have used a genetic complementation strategy to further investigate the *T. brucei* RRP44 nuclease in pre-rRNA maturation. TbRRP44 contains both a PIN and a RNB domain whose homologues are found in association with the exosome complex. We found that the exonucleolytic activity of the RNB domain as well as the physical presence of the PIN domain are essential for TbRRP44 function, while a catalytic site mutation in the PIN domain has no detectable effect on cell growth. A new endonucleolytic cleavage site in ITS1 was identified. In addition to the 5.8S rRNA 3′-end maturation, TbRRP44 is required for degradation of the excised 5′-ETS and for removal of part of ITS1 during maturation of the 18S rRNA 3′-end. TbRRP44 deficiency leads to accumulation of many LSU intermediate precursors, most of them not detected in control cells. TbRRP44 is also required for U3 snoRNA and spliced leader processing, indicating that TbRRP44 may have a wide role in RNA processing in *T. brucei*.**

GRAPHICAL ABSTRACT
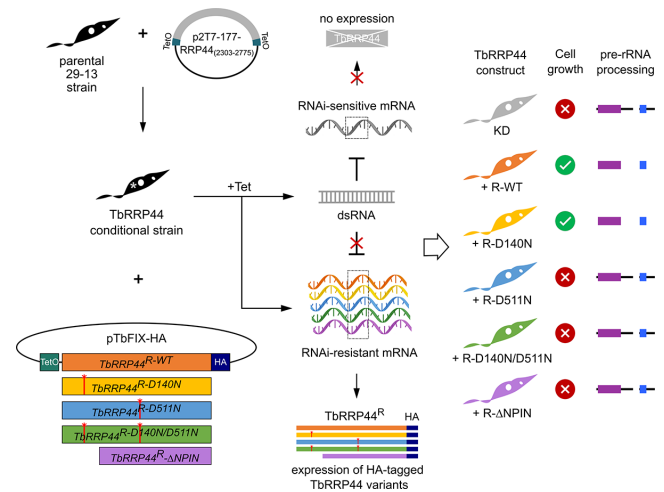
INTRODUCTION

In trypanosomatids, fragmented rRNA in cytoplasmic ribosomes was initially described for *Crithidia fasciculata* (1–3). This feature is shared by the pathogenic trypanosomatids *Trypanosoma brucei*, *T. cruzi* and *Leishmania* sp. In these organisms, the rRNA homologous to the 25S/28S LSU rRNA of other eukaryotes is divided into six fragments, except for *Leishmania* sp. that contains a duplicated segment making a total of seven fragments (4–8). However, fragmented rRNA in cytoplasmic ribosomes is not exclusive from trypanosomatids, which belong to the order Kinetoplastida and share evolutive ancestry with other members of the Phylum Euglenozoa. In this Phylum, *Euglena gracilis* is an extreme example of rRNA fragmentation, which, in addition to the 5.8S rRNA, contains an LSU rRNA split into 13 segments (9,10). Some bacterial species may have intervening spacer sequences in ribosomal RNA genes (11) and fragmented mitochondrial rRNA can also be found especially in apicomplexans, diplonemids and euglenids

*To whom correspondence should be addressed. Tel: +55 41 33163225; Fax: +55 41 3316 3267; Email: nilson.zanchin@fiocruz.br

(12–17). Although this feature was considered reminiscent of primordial ribosomes by some authors (18), the evolution of fragmented rRNA seems more complex. Some bacterial species (19) and some groups of microbial eukaryotes (7) contain self-splicing group I introns in rRNA genes. In addition, the rDNA genes from arthropods can harbor transposable elements that also result in fragmented LSU rRNA (20,21).

A working model for the mechanism of eukaryotic ribosome biogenesis has been initially established in the yeast *Saccharomyces cerevisiae* based both on genetics and biochemical studies (22,23). During ribosome assembly, rRNA folding, excision of spacers sequences and binding of ribosomal proteins is carried out by hundreds of transient ribosome biogenesis factors. Recent Cryo-EM studies describing the structures of the pre-90S (24–26), pre-40S (27–29) and pre-60S (30–32) particles have generally supported the previous model and provided new insights on the specific role of the many ribosome biogenesis factors. rRNA maturation includes also 2′-*O*-methylation and uridine isomerization to pseudouridine at specific sites, which influence ribosome activity (33–36). Although the pre-rRNA processing pathway is generally conserved in all eukaryotes, proteomics studies and gene knockdown screens have revealed higher complexity in the synthesis of human ribosomes relative to *S. cerevisiae*, as well as an intricated interplay with other cellular processes in human cells (37–40). Significant differences in the methylation and pseudouridylation patterns are also observed in human (41,42) and plant cells (43) relative to *S. cerevisiae*. Similarly, approximately 40% of the *T. brucei* rRNA methylation sites are not conserved in *S. cerevisiae*, humans and plants (44).

The structural arrangement of pre-rRNAs containing fragmented rRNA segments of trypanosomatids contrasts with the more compact pre-rRNA structures found in yeast, mammalians, and plants. In these groups, the pre-rRNA comprises 5′ and 3′ external spacer sequences (5′-ETS and 3′-ETS) and two internal spacers (ITS1 and ITS2) separating the sequences that will compose the mature 18S, 5.8S and 25S rRNAs while *T. brucei* pre-rRNA contains a total of seven internal spacers. The *T. brucei* pre-rRNA processing pathway has been reviewed recently by Rajan and coworkers (45). See Figure 1A for details. Presence of extra spacer sequences to be removed from pre-rRNAs implies a more complex mechanism with involvement of a larger number of processing factors or with additional functions played by the factors. Indeed, there is evidence that a larger number of small nucleolar RNAs (snoRNAs) participate in pre-rRNA processing in *T. brucei* (45,46). However, there are few studies on this subject even for the pathogenic trypanosomatids and these mechanisms remain to be investigated.

Most ribosome biogenesis factors function as adaptors to mediate conformational transitions along the pre-rRNA processing steps and ribosome assembly. Nucleolytic processing depends ultimately on a limited number of factors that possess intrinsic catalytic activity (22,23,47,48). The ribosome synthesis factors RRP44 and RRP6 are responsible for most of the 3′-to-5′ exoribonucleolytic activity required for pre-rRNA maturation and degradation of excised spacer sequences. They function in rRNA maturation as catalytic subunits of the exosome complex in *S. cerevisiae*, human and plant cells. RRP6 is found associated to the nuclear exosomes while RRP44 can be found both in cytoplasmic and nuclear exosomes. Both catalytic subunits can bind simultaneously to the complex (49).

RRP44 is a conserved modular protein containing an endoribonuclease PilT N-terminus domain (PIN) and an exoribonuclease module comprising two cold shock (CSD), one RNB and one S1 domains (50–53). The function of the catalytic domains has been investigated in greater detail for the *S. cerevisiae* and human Rrp44p/Dis3 homologues using genetic complementation of catalytic-site and deletion mutants and, *in vitro* RNA degradation assays. In *S. cerevisiae* Rrp44p, replacement of the aspartic acid 551 of the exoribonuclease catalytic site by asparagine (D551N), as well as individual deletion of the cold shock, RNB and S1 domains cause severe growth defect and accumulation of the 7S pre-rRNA and of the excised 5′-ETS segment (50,52–54). Consistently, mutation D551N abolishes the ribonucleolytic activity in vitro (50,54,55). Mutation of catalytic residues of the PIN domain impairs Rrp44p endoribonuclease activity in vitro but has little or no effect on *S. cerevisiae* cell growth (50,52,53). The human RRP44 was also shown to have endoribonucleolytic and exoribonucleolytic activities in vitro that are abolished by mutations in the respective catalytic sites (56). Gene replacement studies using catalytic-site mutant genes resistant to RNA interference showed that the exoribonucleolytic activity is required for maturation of the 5.8S rRNA 3′-end and degradation of the excised 5′-ETS in HEK293 Flp-In T-REx cells (57).

Intriguingly, the trypanosomatid RRP44 was not found in purified exosome complexes, indicating that if an association exists, it must be weak (58–60). Interaction of the *S. cerevisiae* Rrp44p with the exosome complex is mediated by the PIN domain that binds to the exosome ring subunits Rrp41p and Rrp42p (53,61–63). Several structural differences in the *T. brucei* RRP44 (TbRRP44) PIN domain and in the respective TbRRP41 and TbRRP42 homologues may explain the absence of TbRRP44 interaction with the exosome complex (64). Nevertheless, one of the few studies on the *T. brucei* exosome complex showed that in addition to the catalytic subunits TbRRP44 and TbRRP6, the hexameric ring subunits TbRRP41A, TbRRP41B, TbRRP45, and the cap subunits TbCSL4, TbRRP4 and TbRRP40 are required for accurate processing of the 0.61 kb precursor during maturation of the 5.8S rRNA 3′-end (58). Even if not associated, both TbRRP44 and the exosome should cooperate for maturation of the 5.8S rRNA 3′-end.

The crystal structure of TbRRP44 PIN domain confirmed conservation of the catalytic site residues with two manganese atoms as well as the presence of two structural zinc atoms. Previous studies on pre-rRNA processing in *T. brucei* showed that, in addition to the impact in the 0.61 kb pre-rRNA processing (58,64), TbRRP44 depletion also affects maturation of other LSU pre-rRNAs (64). Although the RNAi-mediated depletion of the endogenous TbRRP44 provided evidence on its molecular function, a number of important questions on the role of TbRRP44 catalytic domains in rRNA maturation remain to be investigated.

In this work, we took advantage of the regulated genetic tools available for *T. brucei* RNA interference to develop a
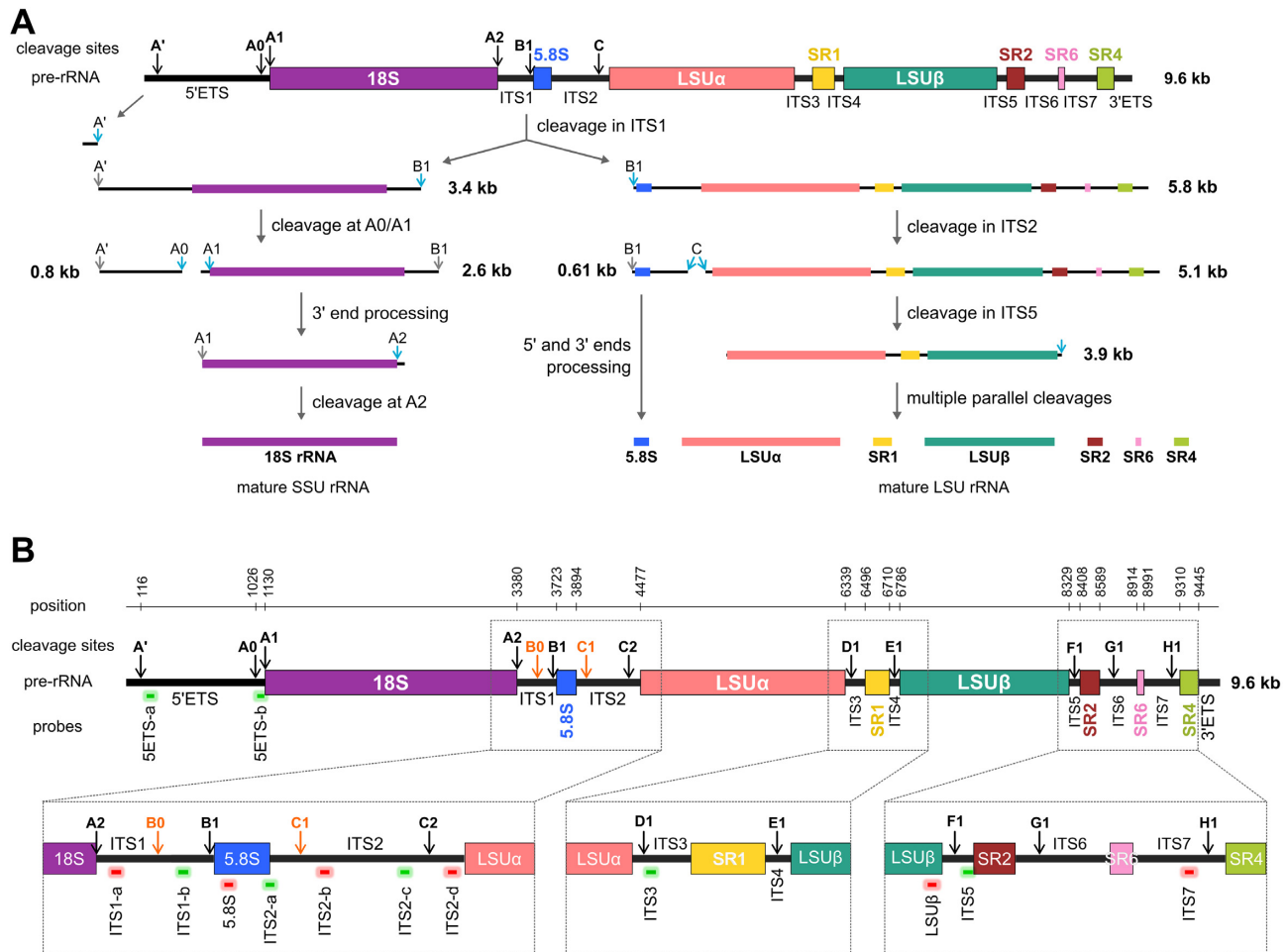
Figure 1. Diagram of *T. brucei* pre-rRNA and major intermediates of its pre-rRNA processing pathway. (**A**) Summary of the previously known *T. brucei* pre-rRNA processing steps. After an initial cleavage at site A', the 9.6 kb pre-rRNA is processed at site B1 in ITS1, separating the 3.4 kb small subunit (SSU) from the 5.8 kb large subunit (LSU) precursors. Subsequent processing of the SSU precursors involves cleavages at sites A0 and A1 for excision of the 5'-ETS, followed by removal of the 3' ITS1 segment and cleavage at site A2 from the 2.6 kb fragment, generating the mature 18S SSU rRNA. The 5.8 kb LSU pre-rRNA is initially cleaved at site C in the ITS2, generating the 0.61 kb and 5.1 kb precursors, followed by a cleavage of the 5.1 kb pre-rRNA in ITS5 generating the 3.9 kb precursor. The 3' segment of the 0.61 kb pre-rRNA is processed by 3'-to-5' RNases to generate the mature 5.8S rRNA. The 3.9 kb is processed in ITS3 and ITS4 to generate the mature LSUα, SR1 and LSUβ. It is unknown if the SR2, SR6 and SR4 pre-rRNAs are processed directly from the 5.1 kb pre-rRNA or if a pre-rRNA containing the SR2, SR6 and SR4 pre-rRNAs is generated by the cleavage of 5.1 kb pre-rRNA at site F1 the generates the 3.9 kb pre-rRNA. Considering that the exact position of the cleavage sites is not known, the sizes of some pre-rRNAs are just approximate. (**B**) Representation of *T. brucei* pre-rRNA structure. The coordinates on the top line indicate the positions of the A', A0 and A1 sites and the 5' and 3' limits of each mature rRNA according to the reference sequence used in this work (GenBank accession: AC159415.1). The diagram shows the positions of the probes (green and red boxes below the diagram) used in this work relative to the positions of the cleavage sites (A' through H1). The new cleavage sites identified in ITS1 and ITS2 are shown in orange.

gene replacement strategy to investigate the function of the individual catalytic domains of TbRRP44. The strategy is based on the use of RNAi-resistant synthetic gene variants to replace the endogenous TbRRP44. This type of strategy has already been successfully used in *T. brucei* studies (65–68) as well as in other systems (57,69). The genetic complementation system has worked as expected to replace the endogenous TbRRP44 by synthetic gene variants. We show that the exonuclease activity of TbRRP44 is essential for *T. brucei* viability. Our results also reveal the requirement of TbRRP44 for accurate processing of the additional spacer sequences of the LSU pre-rRNA, for degradation of the excised 5'-ETS fragment and for removal of part of ITS1 during maturation of the 18S rRNA 3'-end. TbRRP44 is also required for accurate processing of the U3 snoRNA

and of the spliced leader. Mutation of a catalytic residue of the endoribonuclease PIN domain did not affect pre-rRNA processing neither cell proliferation to a detectable level, whereas deletion of the PIN domain caused cell death. In summary, this work provides novel information on pre-rRNA processing and reveals additional details of ribosome synthesis peculiarities in trypanosomatids.

MATERIALS AND METHODS

Genetic complementation strategy

Construction of a *T. brucei brucei* strain derived from strain 29–13 cell line (70) for conditional depletion of the TbRRP44 protein was described in a previous work from our laboratory (64). It carries a 472 bp fragment from the

TbRRP44 gene (nucleotides 2303 to 2775, GenBank accession: AJ308998.1, Supplementary Data, Sequence S1) under the control of two head-to-head T7 RNA polymerase promoters (71). In this construct, transcription of this segment to form double-stranded RNA (dsRNA) is carried out by the phage T7 RNA polymerase, which is under control of the tetracycline repressor/Tet operator pair and induced by tetracycline. The dsRNA triggers the RNA interference (RNAi) response that downregulates TbRRP44 mRNA. To rescue TbRRP44 knockdown, we have used synthetic gene variants that are not recognized by the RNAi machinery. The synthetic gene variants encode the same amino acid sequence of TbRRP44, except for catalytic site mutations and an N-terminal deletion as described below (Supplementary Data, Sequences S2, S3, S6–S13). The region targeted by RNAi shows only 78% nucleotide sequence identity with the wild type gene in the region between nucleotides 2303 and 2775 (Supplementary Data, Sequences S4 and S5). For expression of the synthetic genes resistant to RNAi (RNAi^R), we selected the plasmid pTbFIX, which was shown by Niemirowicz and co-workers (72) to be a tightly inducible system for *T. brucei*. In this plasmid, the sequence of interest is cloned under the control of an rRNA promoter/Tet operator and contains a non-transcribed spacer of the rDNA repeat for directed integration in the *T. brucei* genome after linearization by digestion with the *Not*I restriction enzyme. This regulated system relies on the same genetic tools used for the RNA interference strategy of the *TbRRP44* conditional strain. By using such a combination, depletion of the endogenous TbRRP44 can be synchronized with induction of the *TbRRP44* substitute RNAi^R gene variants. Complementation assays were performed with RNAi^R synthetic genes encoding wild type *TbRRP44* (*TbRRP44^{R-WT}*), an endonucleolytic site mutant (D140N; *TbRRP44$^{R-D140N}$*), an exonucleolytic site mutant (D511N; *TbRRP44$^{R-D511N}$*), a double catalytic site mutant (D140N, D511N; *TbRRP44$^{R-D140N/D511N}$*), and an N-terminal and PIN domain deletion (*TbRRP44^R-ΔNPIN*) comprising amino acid residues 232–972 (numbers according to the GenBank sequence AJ308998.1).

Plasmid constructs for regulated genetic complementation

The plasmid pTbFIX used in this study was kindly provided by Dr León A. Bouvier from the Universidad Nacional de San Martín, Buenos Aires, Argentina. To be able to track expression of the genetic variants, we first inserted a DNA segment encoding the HA tag into the *Xho*I site of pTbFIX to produce plasmid pTbFIX-HA. This DNA segment was isolated from plasmid pMOTag4H (73) using the *Xho*I and *Sal*I restriction enzymes. The *Sal*I site is not reconstituted after ligation with the complementary overhang of the *Xho*I site, leaving a single *Xho*I site for insertion of the coding sequences.

The coding sequence of wild type *TbRRP44* gene resistant to RNA interference (*TbRRP44^{R-WT}*) was obtained as a synthetic gene acquired from GenCust (Boynes, France) cloned into the bacterial expression vector pET28a. The coding sequence of TbRRP44^{R-WT} was transferred to an intermediate plasmid (pComp2, Guerra-Slompo E., unpublished data) using the *Nco*I and *Xho*I restriction sites

and, subsequently, transferred to pTbFIX-HA, using the *Nhe*I and *Xho*I restriction sites while keeping the *Nco*I site for subsequent cloning of the remaining TbRRP44 gene variants to be tested. The resulting plasmid was named pTbFIX-HA-RRP44^{R-WT}.

A second synthetic gene was acquired from BIOMATIK (Kitchener, Ontario, Canada) also cloned into the vector pET28a. It contains the same nucleotide sequence as the TbRRP44^{R-WT}, except for two G-A mutations at nucleotide positions 417 and 1531 (numbers according to GenBank AJ308998.1), which replace aspartic acid codons by asparagine codons, creating endo- and exonuclease catalytic site double mutant. The coding sequence of the double mutant was used to replace the wild type *TbRRP44* coding sequence of pTbFIX-HA-RRP44^R using the *Nco*I and *Xho*I sites to create plasmid pTbFIX-HA-RRP44$^{R-D140N/D511N}$. A *TbRRP44* endonuclease catalytic site single mutant was constructed by fusing the *Nco*I-*Pst*I DNA fragment of the double mutant synthetic gene with the *Pst*I-*Xho*I fragment of the wild type TbRRP44 synthetic gene. Conversely, a TbRRP44 exonuclease catalytic site single mutant was constructed by fusing the *Nco*I-*Pst*I DNA fragment of the wild type TbRRP44 synthetic gene with the *Pst*I-*Xho*I fragment of the double mutant synthetic gene. Both single mutants for the endonucleolytic and exonucleolytic sites were initially constructed in the plasmid pET28a and transferred to pTbFIX-HA using the *Nco*I and *Xho*I sites, replacing the wild-type TbRRP44 coding sequence and creating, respectively, plasmids pTbFIX-HA-RRP44$^{R-D140N}$ and pTbFIX-HA-RRP44$^{R-D511N}$. A deletion construct of *TbRRP44*, termed *TbRRP44^R-ΔNPIN*, lacking the N-terminal and PIN domains and comprising amino acids 232–972 (numbers according to the GenBank sequence AJ308998.1) was acquired from GenCust (Boynes, France) cloned in the *Nco*I and *Xho*I sites of plasmid pET28a. The coding sequence of *TbRRP44^R-ΔNPIN* was inserted into the *Nco*I and *Xho*I sites pTbFIX-HA-RRP44^R, creating plasmid pTbFIX-HA-RRP44^R-ΔNPIN. All constructs and mutations were confirmed by DNA sequencing analysis.

Generation of TbRRP44 conditional derivative strains

T. brucei cultures were maintained as described previously (74). Briefly, *T. brucei* cells were incubated at 28°C in SDM-79 medium containing 10% heat-inactivated bovine fetal serum and the appropriated selective antibiotics (15 μg/ml neomycin, 50 μg/ml hygromycin and 2.5 μg/ml phleomycin). The *T. brucei* strain for conditional depletion of TbRRP44 constructed in the previous work (64) was transfected with the five pTbFIX-HA derivatives each containing a TbRRP44 RNAi^R gene variant (pTbFIX-HA-RRP44^{R-WT}, pTbFIX-HA-RRP44$^{R-D140N}$, pTbFIX-HA-RRP44$^{R-D511N}$, pTbFIX-HA-RRP44$^{R-D140N/D511N}$, pTbFIX-HA-RRP44$^{R-ΔNPIN}$). Transfection was performed with 10–20 μg of *Not*I linearized plasmid DNA and 5×10^7 logarithmic growth phase cells in 100 μl of BSF buffer (5 mM KCl, 0.15 mM CaCl$_2$, 90 mM Na$_2$HPO$_4$, 50 mM HEPES pH 7.3) using a Lonza Nucleofector 2b device (Basel, Switzerland) and program X-001. Subsequently, the cells were suspended in 5 ml of selective medium containing 2 μg/ml puromycin and divided in two populations.

2.5 ml were combined with 2.5 ml of non-transfected cells and 7.5 ml selective medium. Aliquots of 200 μl of this suspension were transferred to 48 wells of 96-well plates. The remaining 2.5 ml of transfected cells was combined to 5 ml of selective medium and cultivated in 25 cm^2 flat-bottom culture flasks. Control cells were treated likewise, excluding addition of plasmid DNA and plating in 200 μl aliquots. The transfected cultures from 96-well plates were incubated for 24 h, diluted 1:2 in selective medium and incubated further for 10 days for selection. The cultures in flasks were harvested whenever they reached exponential growth, until the control cells died due to antibiotic selection. After selection, the clones were expanded and stabilized in 10 μg/ml puromycin prior to characterization. For simplicity, the resulting strains were termed TbRRP44^{R-WT}, TbRRP44$^{R-D140N}$ TbRRP44$^{R-D511N}$, TbRRP44$^{R-D140N/D511N}$ and TbRRP44^{R}-ΔNPIN.

Growth rate analysis of *T. brucei* RRP44 conditional derivative strains

The cultures were synchronized during three passages, prior to induction of RNAi. For growth analysis, *T. brucei* cells were diluted to an initial density of 10^6 cells/ml and 5 ml were transferred to conical 15 ml tubes in triplicates. Induction of both knockdown and complementation was achieved with 2 μg/ml tetracycline on the first day of incubation and 1 μg/ml every 2 days, when the cell density was adjusted to 10^6 cells/ml. Tetracycline was added to the induced conditions only. Every 24 h, the cell number was determined by diluting an aliquot of the culture in PBS and counting using a Beckman Coulter Z2 Cell and Particle counter (Brea, CA, USA). The complementation efficiency of each variant was calculated by dividing the number of cells of induced cultures by the number of cells of the uninduced cultures and represented as percentage with the respective standard deviations of the triplicate averages.

Quantitative reverse transcriptase-PCR

Total RNA was extracted from *T. brucei* cells using the TRIzol™ reagent (Invitrogen-ThermoFisher Scientific, Carlsbad, CA, USA) according to the manufacturer's instructions. RNA samples were quantified on a NanoDrop Spectrophotometer 2000c (ThermoFisher Scientific, Wilmington, DE, USA). cDNA synthesis was performed using the SuperScript IV Reverse Transcriptase kit (Invitrogen-ThermoFisher Scientific, Baltics, UAB, Lithuania) with 2.5 μM random primers following the manufacturer's instructions. cDNAs were diluted to 25 ng/μl and used for qPCR with the SYBR Select Master Mix 2x (Applied Biosystems-ThermoFisher Scientific, Carlsbad, CA, USA). The sequences of the primers used in the RT-qPCR reactions were F-5′-TGTGAAACTCG ATGACACCA-3′ and R-5′-GCGTGTAAATAGGCATG GCA-3′ for the endogenous TbRRP44 mRNA; F-5′-CG AAGAACTGCCGCTGAAAC-3′ and R-5′- CGACTATG CGTAATCGGGCA-3′ for the RNAi-resistant TbRRP44 mRNA; and TbGAPDH_F 5′-AGATTGATGTCGTTG CTGTTGTG-3′ and TbGAPDH_R 5′-ATGGCTTGCTC TTCGTAGTCG-3′ for the GAPDH mRNA. The following programs were used: 95°C for 10 min, 45 cycles of 95°C

for 10 s, 58°C for 10 s (2.2°C/s) and 72°C for 15 s for the primer pair qRRP44^R-F1 and qHAtag-R1, whereas for the endogenous TbRRP44 and TbGAPDH normalizer pairs, annealing was performed at 60°C for 20 s (1°C/s) and extension for 30 s. Reactions were run on the LightCycler 96 from Roche (Basel, Switzerland). The expression levels of experimental triplicates were normalized against GAPDH transcript levels using Pfaffl's equation (75). Each quantification assay was repeated at least one time for validation.

Western blotting

TbRRP44 depletion and expression of the RNAi-resistant variants were confirmed by western blotting with protein extracts of control and tetracycline-induced cells for 48 h. Cells were pelleted by centrifugation at 3000 × *g* for 10 min and washed 3 times with PBS, resuspended 1:1 in PBS and lysis buffer (250 mM Tris–HCl pH 8, 8% SDS, 20% ß-mercaptoethanol, 40% glycerol, 0.04% bromophenol blue) to a final concentration of 10^6 parasites/μl. Cell extracts were incubated at 95°C for 5 min, vigorously shaken for 15 s and centrifuged at 10000 × *g* for 3 min prior to electrophoresis. 5 μl of extracts were separated on 10% SDS-PAGE and transferred to PVDF membranes (GE Healthcare Life Sciences, current Cytiva, Marlborough, MA, USA), which were blocked with 5% fat-free milk in PBS with 0.05% (v/v) Tween 20. Mice polyclonal sera anti-TbRRP44 and anti-TcGAPDH previously obtained (64,76) were used at 1:250 and 1:1000 dilutions, respectively. The HA-tagged variants were detected with a polyclonal rabbit anti-HA at a 1:500 dilution (Invitrogen-ThermoFisher Scientific, Waltham, MA USA). Goat anti-mouse secondary antibody conjugated to IRDye800 CW (cat# 926–32210, LI-COR, Lincoln, Nebraska, USA) and anti-rabbit IgG conjugated to Alexa fluor 680 (cat# A21109, Invitrogen, ThermoFisher Scientific, Waltham, MA USA) were used at 1:15000 and 1:10000 dilutions, respectively. Membranes were incubated with each primary or secondary antibodies for 1 hour at room temperature in PBS with 0.05% Tween 20, under mild agitation. After incubations, membranes were washed 3 times for 5 min. Fluorescent images were acquired on a LI-COR Odyssey scanner (Bad Homburg, Germany).

RNA extraction and northern blots

Induction of both knockdown and complementation was performed as described above in the growth rate analysis section. The cultures, with or without tetracycline treatment, were maintained for 48 h. For each assay condition, ∼4–5 × 10^8 *T. brucei* cells were used for total RNA extraction with the TRIzol™ reagent (Invitrogen- ThermoFisher Scientific, Carlsbad, CA, USA) according to manufacturer's protocol except that the RNA was precipitated with isopropanol at –80°C overnight and collected by centrifugation at 20000 × *g* for 30 min at 4°C, followed by three wash steps with 70% ethanol. After suspension in water, the RNA was quantified on a NanoDrop 2000c spectrophotometer (ThermoFisher Scientific, Wilmington, DE, USA).

For Northern blot analysis of longer rRNA precursors, 8 μg of total RNA were denatured at 65°C for 5 min

Table 1. List of probes used in Northern blot assays

Name	Probe labeling and sequence (5′-3′)	Site of annealing	Complementary rRNA sequence (5′-3′)
5ETS-a	/5IRD700/CCTTAACTGAGGAAGTGTCATACCCAC	5′ETS (141–167)	GUGGGUAUGACACUUCCUCAGUUAAGG
5ETS-b	/5IRD700/TCAAGTGTAAGCGCGTGATCCGCTGTGG	5′ETS (1102–1129)	CCACAGCGGAUCACGCGCUUACACUUGA
ITS1-a	/5IRD800/GGTTGCATACTGTGCAATTATACATGCAC	ITS1 (3416–3444)	GUGCAUGUAUAAUUGCACAGUAUGCAACC
ITS1-b	/5IRD700/GATAGATACGCATTACATACGTATTCTC	ITS1 (3617–3644)	GAGAAUACGUAUGUAAUGCGUAUCUAUC
5.8S	/5IRD800/CGCACTTTGCTGCGTTCTTCAACG	5.8S (3757–3780)	CGUUGAAGAACGCAGCAAAGUGCG
ITS2-a	/5IRD700/TTGTTTTTATATTCGACACTGAGAA	5.8S-ITS2 (3880–3904)	UUCUCAGUGUCGAAUAUAAAAACAA
ITS2-b	/5IRD800/CACTCACTACACACACGTATATGCGTGAC	ITS2 (4044–4072)	GUCACGCAUAUACGUGUGUGUAGUGAGUG
ITS2-c	/5IRD700/CTCTATACGGGGCGCCAAAATACATGCG	ITS2 (4286–4313)	CGCAUGUAUUUUGGCGCCCCGUAUAGAG
ITS2-d	/5IRD800CW/GTGAAGCGTACACGAAAGAAGCAAGCAC	ITS2 (4428–4457)	GUGCUUGUGCUUCUUUCGUGUACGCUUCAC
ITS3	/5IRD700/ACGACAATCACTCACACACACATGGCTAT	ITS3 (6369–6397)	AUAGCCAUGUGUGUGUGAGUGAUUGUCGU
LSUβ	/5IRD800CW/ACATGCCACCGAACGGCAGACCCAGAA	LSUβ (8285–8311)	UUCUGGGUCUGCCGUUCGGUGGCAUGU
ITS5	/5IRD700/AAACACATATACACGTGTGTATAACAGC	ITS5 (8380–8407)	GCUGUUAUACACACGUGUAUAUGUGUUU
ITS7	/5IRD800/TATGTAGTACCACACAGTGTGACGCGCAAC	ITS7 (9154–9183)	GUUGCGCGUCACACUGUGUGGUACUACAUA
7SL	/5IRD800/CCGCCTCGCGACGACACTTGGG	7SL RNA	
U3	/5IRD700/GCTCCTGCCGTTCATCGAACAGCTC	snoRNA U3	
Tb9Cs3C3	/5IRD700/CTCAGACATAGCGCCTCTGTGCAAC	snoRNA Tb9Cs3C3	
Tb10Cs4C3	/5IRD700/ GTACACATTCAAGAGTCCTCATTGG	snoRNA Tb10Cs4C3	
SL	/5IRD700/GCTGCTACTGGGAGCTTCTCATAC	Spliced leader	

in 1.3× loading buffer (60% formamide, 2.5 M formaldehyde, MOPS 1x, 10% (v/v) glycerol, bromophenol blue and 15 μg/ml ethidium bromide) prior to electrophoresis on 1–1.2% agarose-formamide gels in MOPS running buffer at 25–35 V for ∼20 h. Eventually, the MOPS running buffer was replaced by HT buffer (30 mM HEPES, 30 mM triethanolamine) and 0.04 M formaldehyde, which results in a more uniform band separation. After washing the gels for 30 min in H_2O, 20 min in 0.05 M NaOH and 5 min in 20× SSC (SSC 20×: 0.3 M sodium citrate, pH 7.0, 3 M NaCl), capillary transfer blot to nylon membrane (Hybond-N, Amersham, current Cytiva, Little Chalfont, Buckinghamshire, England) was performed using 20× SSC for ∼20 h, followed by membrane air dry and cross-linking on a SpectroLinker™ XL-1500 UV cross-linker (Spectronics Corporation, Westbury, NY, USA). Pre-hybridizations and hybridizations were performed using Church-Gibson modified buffer (0.5 M sodium phosphate pH 7.2, 5% SDS, 1% BSA, 1 mM EDTA) [77] under mild agitation at 42°C for 2 h and 18 h, respectively. Probes were fluorescently labeled with IRDye700 or IRDye800 fluorophores and combined in concentrations ranging from 200 to 500 ng/ml, according to each intensity signal. After hybridization, the membranes were washed twice with 2× SSC, 0.5% SDS and once with 1× SSC, 0.5% SDS at 42°C for 30 min under mild agitation, following additional more stringent washes (reducing SSC and increasing temperature to 50°C) if necessary. Images were acquired on a LI-COR Odyssey scanner (Bad Homburg, Germany) (Supplementary data, Table S1). Band intensities were quantified using the ImageJ software [78].

For Northern blot analysis of shorter precursors, 4 μg of total RNA were fractionated on 4–6% polyacrylamide-8 M urea gels using TBE running buffer (TBE 1x: 89 mM Tris, 89 mM boric acid, 2 mM EDTA pH 8) at 75 V for 3 h. RNA transfer to nylon membranes was performed using a Bio-Rad submerse transfer system (Hercules, CA, USA) in 0.5× TBE for 1 h at 250 mA. Cross-linking and hybridization were performed as described above.

The Northern blot of small nucleolar RNAs was performed as described above, except that different amounts of total RNA were loaded on the 6% polyacrylamide–8 M urea gels. 3 μg of total RNA were used in the Northern blots with the spliced leader and U3 snoRNA probes, and 6

μg were loaded on the gels for the Northern blots with the Tb9Cs3C3 and Tb10Cs4C3 snoRNA probes.

The sequence of the 13 probes used in the northern blot assays are described in Table 1. They were defined based on the rDNA sequence with GenBank accession number AC159415.1 (Supplementary Data, Sequence S14). The positions of the probes relative to the pre-rRNA processing sites on the 9.6 kb primary rRNA precursor are indicated in Figure 1B.

Quantification of precursors using northern blot images

The fluorescence intensity of the distinct rRNA precursors detected by Northern hybridization were quantified using the Gel Analyzer function of ImageJ version 1.52a [78]. The intensity of the area of individual bands from each image was normalized against the mature 18S rRNA of the corresponding ethidium bromide-stained gel. Log_2 transformed ratios of the RNAi-induced samples divided by the respective uninduced samples were plotted on graphs, a procedure mathematically equivalent to the method described by Wang and co-workers [79]. In bar graphs, at least three hybridization replicas were used to calculate the average and standard deviation values for each precursor. Statistical significance was determined using one-way ANOVA followed by Dunnett's multiple comparisons test. For evaluation of the effect of TbRRP44 deficiency on the amount of the LSU and SSU precursors, the intensity of the LSU (5.8 kb) and SSU (3.5 kb) bands detected by probe ITS1-b were determined for each strain in both induced and uninduced conditions and normalized against the mature18S rRNA. The normalized intensities of the 5.8 and 3.5 kb precursors were visualized on a scatter plot. The images used in band quantification are listed in the Supplementary data.

Fluorescent primer extension

Reverse transcriptase primer extension reactions with fluorescently labeled probes were used to identify pre-rRNA cleavage sites. Initially, a rDNA genomic fragment was cloned to be used in sequencing reactions to serve as a molecular size ruler for the primer extension products. For this, genomic DNA was isolated from *T. brucei* cells using a rapid isolation mini-prep method [80]. Briefly, 5×10^7 *T.*

brucei cells were collected by centrifugation, washed in PBS and lysed in 150 μl of TELT solution (50 mM Tris–HCl pH 8, 62.5 mM EDTA pH 8, 2.5 M LiCl, 4% Triton X-100), by gently inverting for 5–10 min at room temperature. The DNA was extracted with phenol:chloroform followed by ethanol precipitation and used as template in PCR reactions to amplify a 1277 bp fragment comprising the last 166 nt of 18S rRNA, ITS1, the 5.8S rRNA and ITS2. The PCR reactions were prepared with Platinum Taq DNA polymerase High Fidelity (ThermoFisher Scientific, Carlsbad, CA, USA), 300 ng of *T. brucei* genomic DNA and 0.4 μM each of the primers ITS1-F (5′-CTGCC ATTTGTACACACCGC-3′) and ITS2-R (5′-GGGTGGT CCTGCCACACTCAGG-3′) following the manufacturers' protocol. The PCR reactions were performed on a ProFlex PCR system (ThermoFischer Scientific, Marsiling, Singapore) using the following conditions: 3 min denaturing at 94°C; 35 cycles of 94°C for 30 s, annealing at 58°C for 20 s and extension at 68°C for 1 min and 10 s, and a final extension for 7 min. The single-band amplification product was purified using the NucleoSpin Gel and PCR Clean-up (MACHEREY-NAGEL, Düren, Germany) and cloned into pGEM-T Easy (Promega, Madison, WI, USA). Three clones were sequenced (pGEM-ITS1/2-C12, pGEM-ITS1/2-C14 and pGEM-ITS1/2-C16), which showed some variation in the ITS1 and ITS2 regions (See supplementary Figure S2 for the variation in ITS1). Clone pGEM-ITS1/2-C14 was used in the sequencing reactions to serve as size reference for the primer extension products.

For the primer extension reactions, 15 ng of the 5.8S-IRD800 probe were mixed to 10 μg of total RNA extracted from uninduced and 48 h-tetracycline induced TbRRP44 knock-down *T. brucei* cells in the presence of the SuperScript IV Reverse Transcriptase buffer (Invitrogen-ThermoFisher Scientific, Baltics, UAB, Lithuania) in 0.2 ml tubes and a final volume of 10 μl. Annealing of the probe to the template was achieved by incubating in a water bath at 95°C for 2 min followed by slow decay to room temperature for ~1.5 h. 10 μl of the extension reaction mixture containing SuperScript IV Reverse Transcriptase, reaction buffer, 0.75 mM dNTP, 5 mM DTT and 40 U RNase OUT (Invitrogen-ThermoFisher Scientific, Carlsbad, CA, USA) and 1x reaction buffer were added to the annealing reaction and incubated at 45°C for 1 h, followed by reaction inactivation at 80°C for 5 min.

For DNA sequencing, plasmid pGEM-ITS1/2-C14 was linearized by digestion with the *Spe*I restriction enzyme and purified with the NucleoSpin kit (MACHEREY-NAGEL, Düren, Germany). DNA sequencing reactions were performed using 1.4 μg of *Spe*I-digested pGEM-ITS1/2-C14 DNA, 60 ng of 5.8S-IRDye800 probe and the Thermo Sequenase Cycle Sequencing Kit (Cat# 78500, Affymetrix – ThermoFisher Scientific, Cleveland, OH, USA), following the basic manufacturer's instructions.

Both the primer extension products and the sequencing reactions were mixed with 1 volume sample buffer (95% formamide, 10 mM EDTA pH 8), denatured at 75°C for 2 min and separated on 8% polyacrylamide-7 M urea gels (dimensions 20 cm × 20 cm × 0.4 mm) in TBE buffer at 500 V for 2 h and 40 min (<100 bp products) or 4 h and 30 min (>100

bp products). Fluorescence gel images were acquired on a LI-COR Odyssey scanner (Bad Homburg, Germany).

RESULTS

Rescue of RNAi-mediated knockdown of endogenous TbRRP44 by an RNAi-resistant copy of the TbRRP44 gene

The plasmid pTbFIX described by Niemirowicz and co-workers (72) was used for expression of wild type and mutants of TbRRP44 in the complementation assays. pTb-FIX combines sequences that drive transcription activity and a minimum set of regulatory components. In this vector, the sequence of interest is cloned under the control of an rRNA promoter/Tet operator, which is strongly induced by doxycycline/tetracycline in both bloodstream and procyclic *T. brucei* forms (72). Initially, we modified the original pTbFIX vector to include a sequence encoding the HA tag downstream to the restriction sites for gene cloning, thus allowing to obtain proteins with a C-terminal HA-fusion tag, for distinction of the endogenous from the heterologous proteins. Subsequently, we cloned a RNAi-resistant synthetic copy of the wild type TbRRP44 gene in the modified pTbFIX vector and transfected the resulting plasmid (pTbFIX-HA-RRP44^{R-WT}) into a *T. brucei* strain for conditional TbRRP44 depletion, which was constructed in a previous work (64).

After selection of transfectants, several clones carrying the TbRRP44^{R-WT} variant were tested for rescue of the growth phenotype by tetracycline induction in parallel with the parental conditional strain as a control. The TbRRP44^{R-WT} clones show highly similar growth rates both with and without tetracycline induction while growth of the TbRRP44 parental conditional strain starts to decrease after 24 h and stops after 2 days of RNAi induction (Figure 2A, B). Quantification of the mRNA levels confirmed the reduction of the endogenous TbRRP44 mRNA and revealed a 4–5-fold increase in the TbRRP44^{R-WT} mRNA (Figure 2C). Consistently, the protein encoded by TbRRP44^{R-WT}, containing a C-terminal HA tag, was detected by Western blot using an anti-HA antibody (Figure 2D). No TbRRP44^{R-WT} protein was detected in uninduced cells, showing that there is no leakage of the regulated expression system without tetracycline (Supplementary Data, Figure S1). The growth rate of the clones rescued by the RNAi-resistant gene upon tetracycline treatment is similar to the rate of uninduced parental cells, indicating that the HA-tag is not deleterious for TbRRP44 function. In addition, this shows that integration of pTbFIX carrying TbRRP44^{R-WT} in the non-transcribed spacer of the rDNA repeat did not affect cell growth. Overall, these results confirm efficient complementation of the endogenous TbRRP44 mRNA knockdown by the synthetic gene using the pTbFIX-HA-RRP44^{R-WT} construct.

Evaluation of the rescue of TbRRP44 knockdown by RNAi-resistant TbRRP44 mutants

After demonstrating that the wild type *TbRRP44* RNAi-resistant synthetic gene (*TbRRP44^{R-WT}*) was able to complement the conditional strain concomitantly with
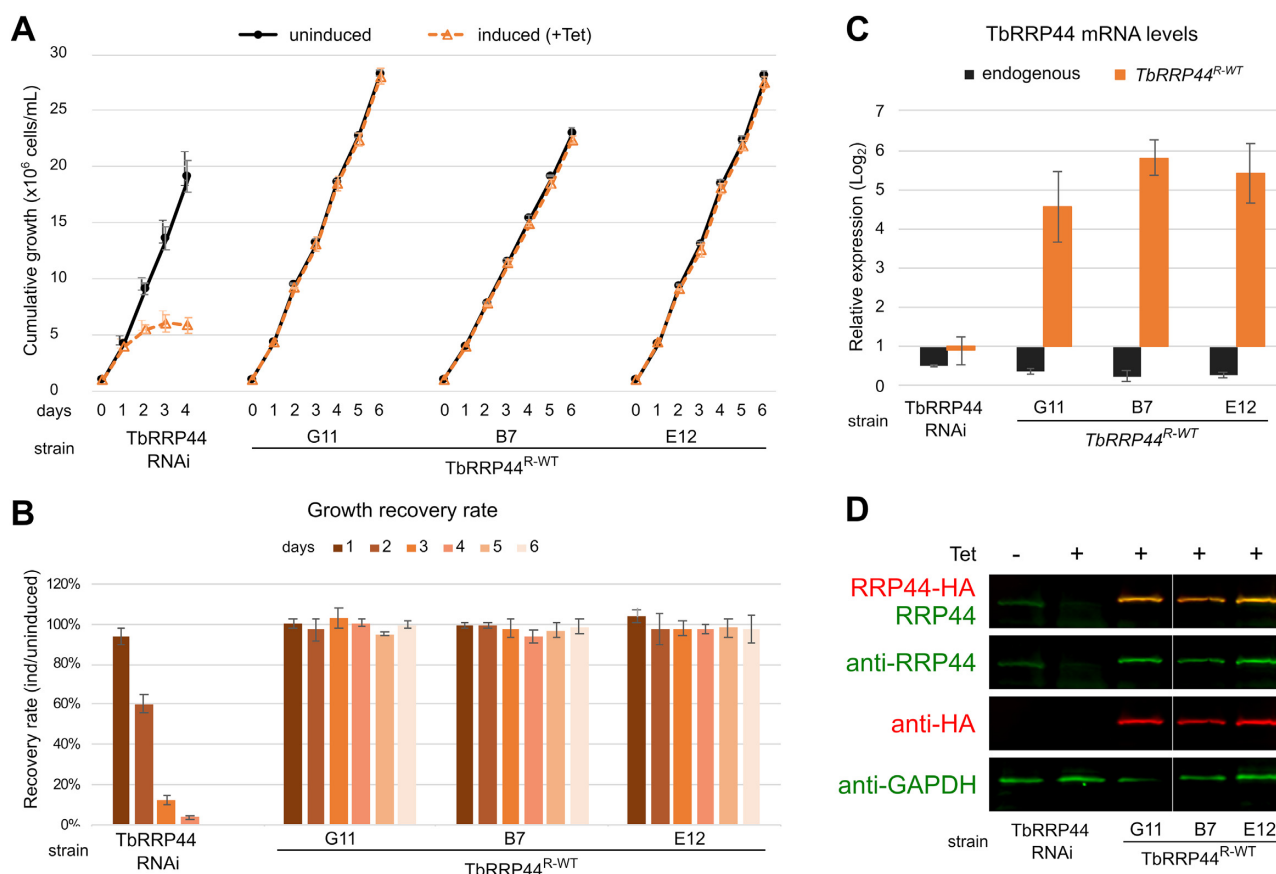
Figure 2. Complementation of the endogenous TbRRP44 knockdown by an RNAi-resistant copy of the wild type TbRRP44 gene (TbRRP44R^{WT}). (**A**) Growth curves of three clones expressing TbRRP44^{R-WT} compared to the TbRRP44 conditional strain. The curves represent the average number of *T. brucei* cells per ml of cultures performed in triplicate with the respective standard deviation, during six days in presence (Induced/Tet+) or absence (Uninduced) of tetracycline, with daily cell count and culture dilution back to 10^6 cells/ml every second day. (**B**) Cell number ratio of the tetracycline-induced vs. uninduced cultures shown in (A). Colored bars represent the average number of cells of the triplicates and the respective standard deviation. (**C**) TbRRP44 mRNA levels from cultures induced with tetracycline for 2 days relative to cultures not treated with tetracycline as determined by quantitative RT-PCR normalized against TbGAPDH. The reactions were performed in triplicates and repeated at least twice. The y axis shows the normalized average of TbRRP44 mRNA levels with the respective standard deviation. (**D**) Analysis of knockdown of the endogenous TbRRP44 protein and expression of TbRRP44^{R-WT}. Western blots were performed using whole-cell extracts and polyclonal antisera against TbRRP44 (anti-RRP44), HA tag (anti-HA) and GAPDH (anti-GAPDH) as a loading control (bottom panel). The upper panel shows an overlay of the two Western blots. The anti-TbRRP44 polyclonal serum (green) detects the TbRRP44 protein in uninduced cell extracts of the parental conditional strain and the TbRRP44 expressed by the RNAi-resistant clones, while the anti-HA antibody (red) detects only the HA-tagged TbRRP44 expressed by the RNAi-resistant clones.

knockdown of the endogenous TbRRP44, we tested the strains transfected with plasmids pTbFIX-HA-RRP44$^{R-D140N}$, pTbFIX-HA-RRP44$^{R-D511N}$, pTbFIX-HA-RRP44$^{R-D140N/D511N}$ and pTbFIX-HA-RRP44^R-ΔNPIN. The TbRRP44 conditional strain and the strain carrying TbRRP44^{R-WT} were tested in parallel as controls. The growth rate of the strain expressing TbRRP44$^{R-D140N}$ was similar to the strain carrying TbRRP44^{R-WT} (Figure 3A, B), indicating that replacement of aspartic acid 140 by asparagine (D140N) in the endonuclease catalytic domain has no detectable effect on cell growth. However, the strain carrying TbRRP44^R-ΔNPIN, with deletion of the N-terminal and NPIN domain, shows a reduction in the growth rate similar to the parental conditional strain and, eventually stops growing completely (Figure 3A, B). This finding indicates that while lack of endonuclease activity does not affect cell growth above

a measurable threshold, presence of the NPIN domain is essential for *T. brucei* viability. The cells carrying the exonucleolytic domain mutant (TbRRP44$^{R-D511N}$) and both catalytic site mutants (TbRRP44$^{R-D140N/D511N}$) also show growth inhibition similar to the parental conditional strain and stop growing (Figure 3A, B). Analysis of the mRNA and protein levels of the strains carrying plasmids pTbFIX-HA-RRP44$^{R-D140N}$, pTbFIX-HA-RRP44$^{R-D511N}$, pTbFIX-HA-RRP44$^{R-D140N/D511N}$ and pTbFIX-HA-RRP44^R-ΔNPIN confirmed expression of the respective TbRRP44 mRNA and protein variants after induction with tetracycline (Figure 3C, D), showing that reduction of growth rate is not due to lack of protein expression. These results indicate that the catalytic activity of the exonucleolytic domain as well as the presence of the PIN domain are essential for TbRRP44 protein function.
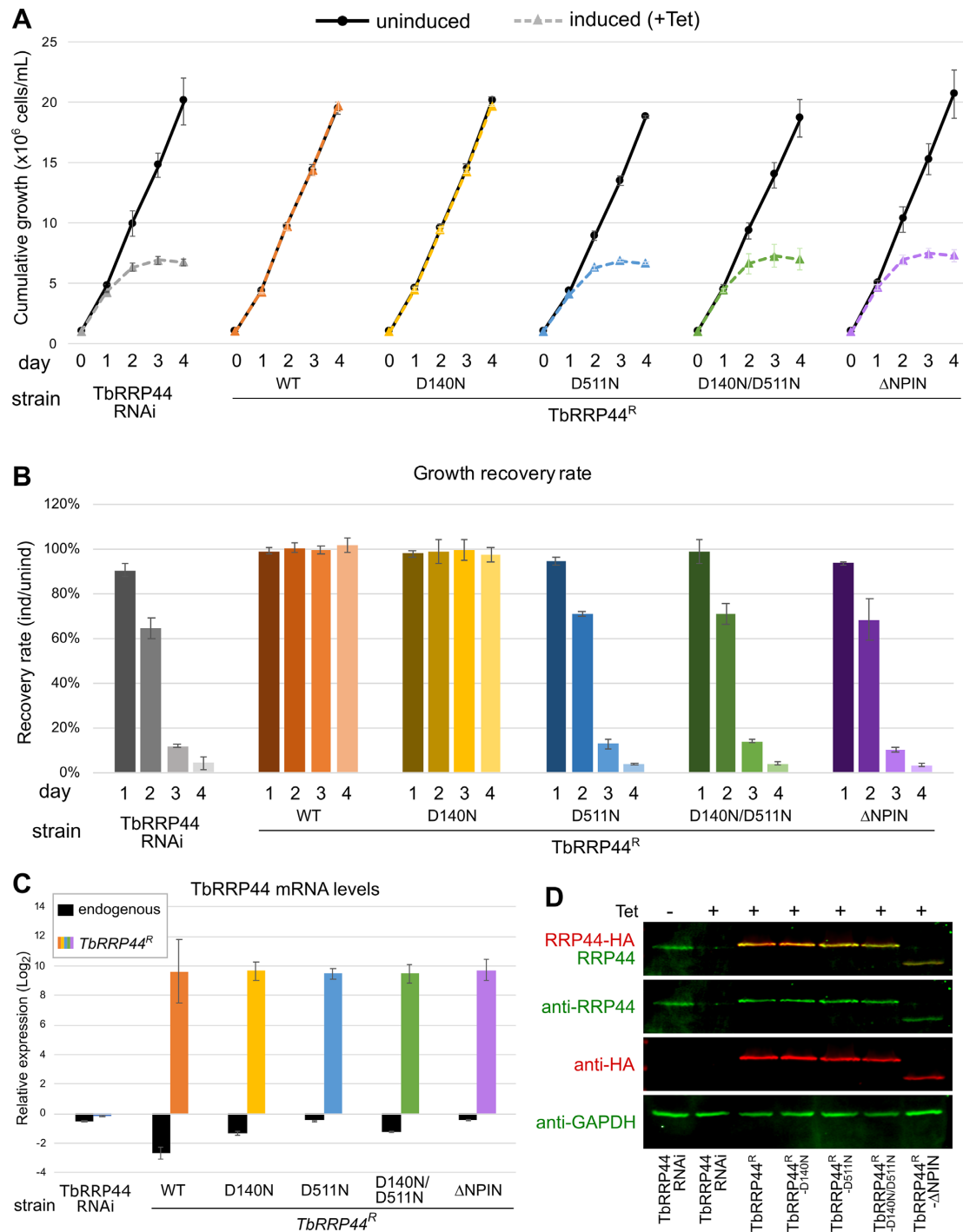
Figure 3. Evaluation of the complementation of TbRRP44 knockdown by RNAi-resistant TbRRP44 mutants. (**A**) Growth rate of strains transfected with the rescue plasmids pTbFIX-HA-RRP44^{R-WT}, pTbFIX-HA-RRP44$^{R-D140N}$, pTbFIX-HA-RRP44$^{R-D511N}$, pTbFIX-HA-RRP44$^{R-D140N/D511N}$, pTbFIX-HA-RRP44^{R}-ΔNPIN. The curves represent the average number of *T. brucei* cells per ml of cultures performed in triplicate with the respective standard deviation, during four days in presence (Induced/Tet+) or absence (uninduced) of tetracycline, with dilution back to 10^6 cells/ml every second day. (**B**) Cell number ratio of the tetracycline-induced vs. uninduced cultures shown in (**A**). Colored bars represent the average number of cells of the triplicates and the respective standard deviation. The TbRRP44$^{R-D140N}$ mutant does not show growth phenotype while the TbRRP44$^{R-D511N}$, TbRRP44$^{R-D140N/D511N}$ and TbRRP44^{R}-ΔNPIN show growth phenotypes similar to the parental conditional strain. (**C**) Quantitative RT-PCR determination of the TbRRP44 mRNA levels from cultures induced with tetracycline for 2 days relative to cultures not treated with tetracycline normalized against TbGAPDH. The reactions were performed in triplicates and repeated at least once. The y axis shows the normalized average of TbRRP44 mRNA levels with the respective standard deviation. (**D**) Analysis of expression of the TbRRP44 mutant proteins encoded by the RNAi-resistant genes. Western blots of cell extracts were performed using polyclonal antisera against TbRRP44 (anti-RRP44), HA-tag (anti-HA), and GAPDH (anti-GAPDH) as a loading control (bottom panel). The upper panel shows an overlay of the Western blots performed with the anti-TbRRP44 polyclonal serum (green) that detects TbRRP44 in uninduced cells of the parental conditional strain and the wild type TbRRP44 and the mutants expressed by the RNAi-resistant genes, while the anti-HA antibody (red) detects only HA-tagged TbRRP44 expressed by the RNAi-resistant genes.

Early processing of the 9.6 kb primary rRNA precursor and identification of a new ITS1 cleavage site

Previous studies have shown the requirement of TbRRP44 function for accurate processing of the 7S pre-rRNA and other precursors of the large ribosomal subunit in *T. brucei* cells (58,64). In this work, we have analyzed the specific role of catalytic residues of the endonuclease and exonuclease domains, as well as the role of the NPIN domain of TbRRP44 for maturation of *T. brucei* ribosomal RNA. For this purpose, we performed Northern blots with a set of 13 probes complementary to different positions in the pre-rRNA (Table 1 and Figure 1B). The probes are labeled with two different chromophores to facilitate identification of the many intermediate precursors with similar sizes that are generated by processing of the highly segmented *T. brucei* pre-rRNA.

The levels of the 9.6 kb primary rRNA precursor were at the limit of the detection for all fluorescent probes used (Figures 4 and 6). This indicates that the 9.6 kb pre-rRNA is quickly processed, generating the so-called 3.5 kb SSU and 5.8 kb LSU precursors described in previous studies on *T. brucei* pre-rRNA processing (reviewed in (45)). In control cells, the probes hybridizing in the 5′-ETS (5ETS-a, 5ETS-b) and near the 3′-end of the mature 18S rRNA (ITS1-a) detected only the 3.5 kb as a major SSU precursor (Figure 4). Surprisingly, probe ITS1-b, which hybridizes in ITS1 in a different position relative to the probes used in previous studies, detected both the 3.5 kb SSU precursor and the 5.8 kb LSU precursors (Figures 4B and 6A). This finding shows that approximately half of the SSU and the LSU precursors contain the same ITS1 segment comprising the region of probe ITS1-b. This indicates the existence of two endonucleolytic cleavage sites within ITS1, one upstream and another downstream of the probe ITS1-b (Figure 4D). More importantly, as in the case of mouse ITS1 processing (79), presence of both SSU and LSU precursors with extensions comprising the region of the probe ITS1-b indicates that the two cleavages in ITS1 do not take place simultaneously. Presence of two cleavages sites is also consistent with the different band pattern shown by probe ITS1-b relative to the Northern blots performed with probes ITS1-a and 5.8S (see below). This is a new finding since previous studies reported only one cleavage site in ITS1 located near the 5′-end of the 5.8S rRNA, usually identified as cleavage site B1 (45,46,81–84). The new site is located at the segment between probes ITS1-a and ITS1-b. Since the new site is located upstream the previously known site B1, it was tentatively named 'B0' throughout this work (Figure 4D).

A more precise mapping of the position of the B0 cleavage site was performed using primer extension. Several probes were tested, and best results were obtained with probe 5.8S labeled with chromophore IRDye800. Three major primer extension products were detected although the two products of lower molecular weight differ by a single nucleotide only (Figure 5A). These two products migrate at the expected position for the 5′ end of the mature 5.8S rRNA. In control cells, the product terminating at cytosine -1 shows a more intense signal while a weaker band is observed for the product ending at the adenosine +1 relative to the ma-

ture 5.8S rRNA 5′ end. These twin bands, however, showed similar intensities in the TbRRP44 knockdown cells (Figure 5A, C). The position of product showing higher molecular weight was mapped to nucleotide –136, a cytosine, according to the dideoxynucleotide sequencing ladder generated by sequencing the ITS1 region and should correspond to the cleavage site B0 (Figure 5B, C). In TbRRP44 knockdown cells, this primer extension product shows a stronger signal indicating that processing of the precursor cleaved first at site B0 may be affected by TbRRP44 deficiency. It is important to point out, however, that different *T. brucei* rDNA copies present a considerable degree of variation in ITS1 (see Supplementary Figure S2). Therefore, the specific position of the cleavage site may vary according to each specific rDNA copy. This cytosine is located at position –136 relative to the 5.8S rRNA 5′-end based on the sequence obtained from plasmid pGEM-ITS1/2-C14 sequenced in this work. Considering the variations between the rDNA repeats, this cytosine is located at position –140 of the sequence with GenBank accession number AC159415.1.

Concerning site B1, other than the 5′-end of the mature 5.8S, the primer extension analyses did not reveal a clear primer extension product for the expected position of the B1 processing site. Initial processing of *T. brucei* primary pre-rRNA has been proposed to initiate at site B1 near the ITS1/5.8S boundary (45,46,84,85). This would be consistent with the data obtained in this work. However, a study published by Sakyiama and co-workers (86) using a probe that hybridizes exactly in the ITS1/5.8S boundary has identified a 5′ extended 0.17 kb form of the 5.8S rRNA that accumulates in XRNE-deficient cells. This indicates that the 5′ site of the 5′ extended 5.8S rRNA could correspond to site B1. Therefore, we expected to detect a primer extension product upstream the 5′-end of the mature 5.8S rRNA and downstream of probe ITS1-b. Instead, only sequentially weaker products are observed up to the positions -5/-6, and at -12 and -19 upstream of the major bands that correspond to the 5′ end of the mature 5.8S rRNA (Figure 5A). If site B1 is not located exactly at the ITS1/5.8S rRNA boundary, possibly after cleavage at site B1, the 5′ end of the LSU precursor is quickly processed by 5′-to-3′ nucleases, so that a discrete primer extension product cannot be detected by the method used in this work.

Based on the positions of cleavage site B0, probe ITS1-b and of the 5.8S rRNA 5′-end, the difference between the two types of LSU precursors in the 5′ region would be of at least 58 nucleotides and at most 140 nucleotides (see Supplementary Sequence S14). Therefore, we will refer to the LSU cleaved at site B0 as LSU-B0 and 5.8 kb, and LSU-B1 and 5.7 kb for the LSU cleaved at site B1. The 5.8 and 5.7 kb sizes, however, are estimated considering the position of the B0 and B1 sites and the 3′-end of SR4 and should be taken as just approximate estimations since the position of the 3′ of these pre-rRNAs has not been defined.

SSU pre-rRNA processing defects in TbRRP44-deficient cells

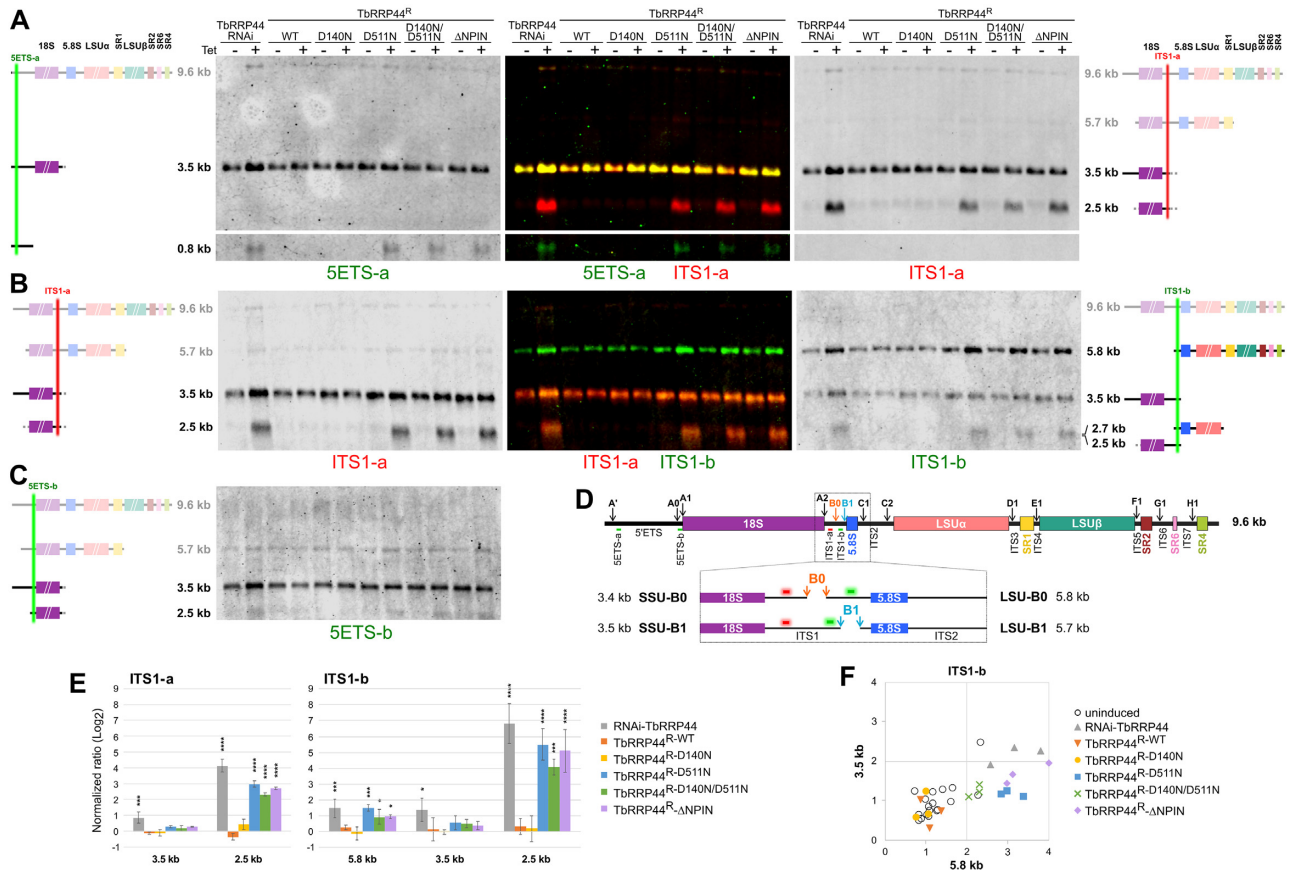In control cells, the Northern analyses revealed only the 3.5 kb, corresponding to the SSU rRNA precursor as a

Figure 4. Analysis of SSU pre-rRNA processing by Northern blots using probes complementary to the 5′-ETS and ITS1. The TbRRP44 variants are identified at the top and probes at the bottom of each panel, respectively. Cultures untreated and treated with tetracycline (Tet) are indicated by – and +, respectively. Diagrams of the parts that compose each pre-rRNA fragment detected by each probe are indicated at the left and right sides of the images. The precursors detected at lower levels are indicated in fainter colors. Green and red vertical lines on the diagrams indicate the position of the probes on each pre-rRNA intermediate. The central panels show an overlay of the two blots. Green and red bands indicate the precursors detected only by the probe on the left or on the right, respectively. Orange/yellow indicates the precursors detected by both probes. (**A**) Northern blots performed with probes 5ETS-a (left) and ITS1-a (right). Both probes detect the 3.5 kb SSU pre-rRNA. In addition, probe 5ETS-a detects a 0.8 kb fragment of the excised 5′-ETS and, probe ITS1-a detects a 2.5 kb band in parental TbRRP44 KD cells and in cells expressing non-complementing TbRRP44 mutants. (**B**) Northern blots performed with probes ITS1-a and ITS1-b. Probe ITS1-a detected the same bands as in (**A**). Probe ITS1-b detected both the 3.5 kb SSU precursor and the 5.8 kb LSU precursor, resulting from two non-simultaneous cleavage sites in ITS1. This probe also detects a band in the range of 2.5/2.7 kb in parental KD cells and in cells expressing non-complementing TbRRP4 mutants. (**C**) Northern blot performed with probe 5ETS-b, complementary to the 5′-ETS between site A0 and A1. This probe detects a major band corresponding to the 3.5 kb SSU pre-rRNA and two weak bands of ∼5.7 and 2.5 kb. The latter is detected only in the cells with knockdown or functionally deficient TbRRP44. (**D**) Diagram showing in detail the position of the B0 and B1 endonucleolytic cleavage sites relative to the probes ITS1-a and ITS1-b with the respective SSU and LSU fragments generated. (**E**) Graphs showing the ratio of precursors between tetracycline-induced and uninduced control cells detected with probes ITS1-a (left) and ITS1-b (right). Statistical significance was tested for the intensity of the precursors in cells defective for TbRRP44 relative to the intensity of the same precursor in the cells complemented by TbRRP44^{R-WT}, using one-way ANOVA followed by Dunnett's multiple comparisons test. * p ≤ 0.05, *** $P ≤ 0.001$, **** $P ≤ 0.0001$. (**F**) Scatter plot of the LSU (5.8 kb) and SSU (3.5 kb) normalized intensities generated by probe ITS1-b from three Northern blots. After knockdown of the endogenous TbRRP44, parental TbRRP44 KD cells and cells expressing the non-complementing TbRRP4 mutants show higher values for the 5.8 kb LSU pre-rRNA intensities.

major band (Figure 4A–C, 'Tet–' lanes). In these cells, an additional weak band in the range of 5.7 kb is also detected by probes 5ETS-b and ITS1-a but not by probe 5ETS-a. Given the position of these probes, this 5.7 kb band does not correspond to the same 5.7 kb LSU-B1 pre-rRNA. Instead, it most probably corresponds to a product of a secondary pathway, spanning from site A0 up to site E1 in ITS4 (estimated size of 5.7 kb) (Figure 4A, right panel, 4B and 4C left panel). A pre-rRNA intermediate with this size would be also detected by probe ITS1-b but it would comigrate with the 5.8 kb band detected by this probe. Comparatively, probe ITS1-a seems to be a little more sensitive

than the others since it detected trace amounts of a 2.5 kb SSU pre-rRNAs (2.5 kb/A0-B0/A0-B1/A1-B0/A1-B1) in control cells (Figure 4A, B).

A different scenario is observed in the strains that do not complement the knockdown of the endogenous TbRRP44 under RNAi-induced conditions (Figure 4A–C, 'Tet+' lanes). Under non-permissive conditions, the pre-rRNA processing defects were identical for both the parental conditional strain and for the strains carrying the TbRRP44$^{R-D511N}$, TbRRP44$^{R-D140N/D511N}$ and TbRRP44^{R}-ΔNPIN variants. For clarity, the pre-rRNA processing defects will be described collectively for these
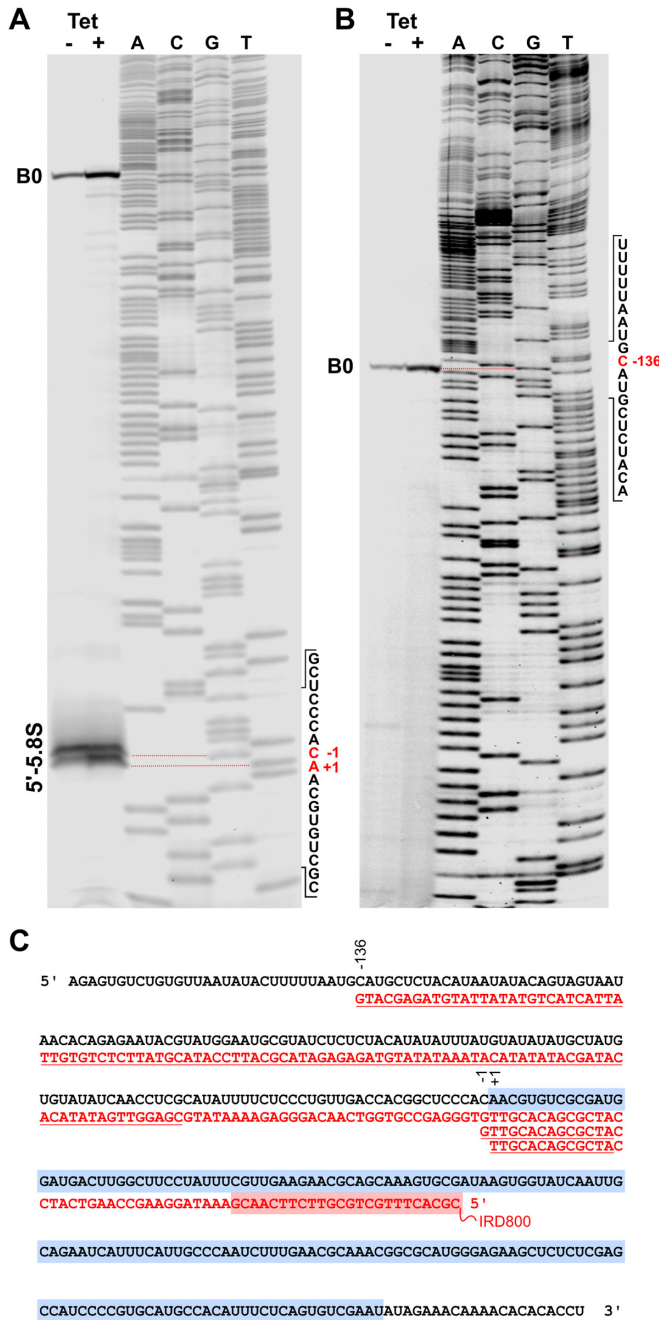
four strains when incubated in the presence of tetracycline for knockdown of the endogenous TbRRP44 and expression of the TbRRP44$^{R-D511N}$, TbRRP44$^{R-D140N/D511N}$ and TbRRP44^R-ΔNPIN variants.

TbRRP44 deficiency led to the accumulation of a fragment of ∼0.8 kb, corresponding to the excised 5′-ETS segment (Figure 4A, probe 5ETS-a), and of the 2.5 kb SSU pre-rRNAs comprising the 18S rRNA and part of ITS1 (2.5 kb/A0-B0/A0-B1/A1-B0/A1-B1; Figure 4A-C, probes 5ETS-b, ITS1-a and ITS1-b). However, it is important to note that, as described below, in TbRRP44 deficient cells probe ITS1-b can also detect a 2.7 kb fragment of the LSU pre-rRNA, comprising from site B0 up to the site D1 (2.7 kb/B0-D1). Due to the low resolution of the agarose gel electrophoresis, both precursors are expected to co-migrate in a single band and would not be distinguished in the Northern blot with probe ITS1-b and are indicated as overlapping bands in Figure 4B (right panel).

In addition, TbRRP44 deficiency affected the ratio between the amounts of the 5.7–5.8 kb LSU and 3.4–3.5 kb SSU precursors. This was confirmed by analysis of the ratio between the 5.7–5.8 kb LSU and 3.4–3.5 kb SSU precursors detected with probe ITS1-b. The cells incubated under permissive conditions and the cells expressing TbRRP44^{R-WT} and TbRRP44$^{R-D140N}$ present similar 5.8 kb/3.5 kb ratios. On the other hand, the cells expressing the mutants TbRRP44$^{R-D511N}$, TbRRP44$^{R-D140N/D511N}$ and TbRRP44^R-ΔNPIN show an increase in the ratio between the 5.8 and 3.5 kb precursors (Figure 4E, F). This indicates that, upon knockdown of the endogenous TbRRP44 and induction of the non-complementing mutants, there may be either an increase in the ITS1 cleavage in site B0 relative to site B1 or a slower processing of the LSU precursor cleaved at site B0. In the parental conditional strain, however, knockdown of TbRRP44 seems to lead to a small increase also in the SSU precursor (Figure 4E, F).

LSU pre-rRNA processing defects in TbRRP44-deficient cells

The Northern analyses with all probes that hybridize downstream to the 5.8S rRNA 5′-end revealed a single major LSU precursor in control cells (Figures 6, 7, 'Tet –' lanes). However, considering the cleavages at sites B0 and B1 separating the SSU from the LSU precursors, the LSU seen in the blots must comprise the two types, the LSU-B0/5.8 kb, and the LSU-B1/5.7 kb. Precursors of 5.1 kb and 0.7 kb

Figure 5. Primer extension analysis of ITS1 processing sites. Lanes – and + indicate the primer extension products of reverse transcriptase reactions performed with probe 5.8S-IRDye800 and RNA extracted from *T. brucei* cells uninduced (Tet–) and from cells induced with tetracycline (Tet+) for 48 h. A, C, G, T, indicate a dideoxynucleotide sequence ladder generated by DNA sequencing using the same probe and a DNA template containing the ITS1, 5.8S rRNA and ITS2 segment, which was run in parallel on 8% polyacrylamide-7 M urea gels. (**A**) Analysis of primer extension products after a 2 h and 40 min electrophoresis time. Two products of lower molecular weight differ by a single nucleotide and migrate at a position that should correspond to the 5′ end of the mature 5.S rRNA. In control cells, the product terminating at cytosine –1 is more intense while a weaker band is observed at adenine + 1 relative to the 5.8S rRNA 5′ end of the sequence used in this work derived from plasmid pGEM-ITS1/2-C14. Both bands show similar intensities in TbRRP44 knockdown cells. (**B**) Analysis of primer extension products as described in (A) except that the electrophoresis was run for 4 h and 30 min to better resolve the dideoxynucleotide se-

quence ladder in the range of the larger primer extension product. This product was mapped to cytosine -136 and should correspond to the cleavage site B0. The position of this cytosine is according to the ITS1 sequence obtained from plasmid pGEM-ITS1/2-C14. (**C**) Sequence detail showing the position of the primer extension products identified with probe 5.8S-IRDye800 probe (red box). The blue box indicates the mature 5.8S rRNA segment. The partial DNA sequence obtained from the dideoxynucleotide sequencing of plasmid shown pGEM-ITS1/2-C14 in (A) and (B) is represented in red underneath the respective segment of the pre-rRNA sequence. The underlined regions correspond to the sequence segments obtained directly from the sequencing reactions shown in this figure. The positions of the ends of the primer extension products are indicated as + 1, –1 and –136 relative to the 5′ end of the 5.8S rRNA according to the ITS1 sequence obtained from plasmid pGEM-ITS1/2-C14.
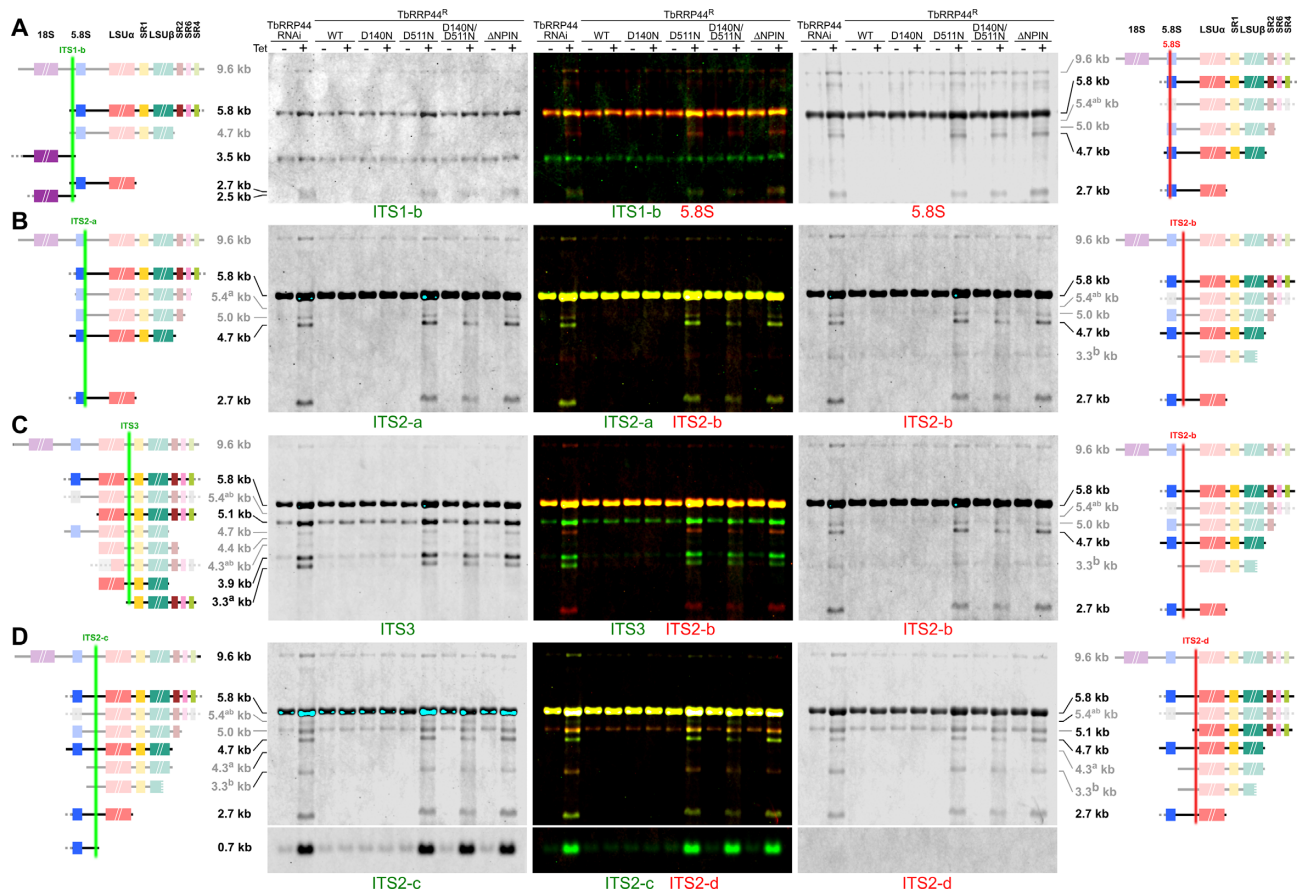
Figure 6. Analysis of LSU pre-rRNAs by Northern blots with probes hybridizing in the 5.8S rRNA and in ITS2. Northern blots with probes ITS1-b and ITS3 are also shown for comparison. Diagrams of the parts that compose the precursors detected by each probe are indicated at the left and right sides of the images. The pre-rRNAs detected at lower levels are indicated in fainter colors. The diagrams of the precursors 5.4^{ab} kb and 4.3^{ab} kb for which the 5′ and 3′ boundaries could not be assigned are marked in grey. Green and red vertical lines on the diagrams indicate the relative position of the probes on each pre-rRNA intermediate. In the Northern blot images, probes are identified at the bottom and the TbRRP44 variants at the top of each panel, respectively. Cultures untreated and treated with tetracycline (Tet) are indicated by – and +, respectively. The central panel shows an overlay of the two blots. Green and red bands indicate the precursors detected only by probe on the left or on the right, respectively. Orange/yellow indicates the precursors detected by both probes. (**A**) Northern blots performed with probes ITS1-b (left) and 5.8S (right). (**B**) Northern blots performed with probes ITS2-a (left) and ITS2-b (right). (**C**) Northern blots performed with probes ITS3 (left) and ITS2-b (right). (**D**) Northern blots performed with probes ITS2-c (left) and ITS2-d (right). The Northern blot with probe ITS2-a was performed on the same membrane as the Northern blot for probes ITS2-b and ITS3 after stripping the probes of the first hybridization. Therefore, the same ITS2-b image is used in the overlay with probes ITS2-a and ITS3. In control cells (lanes Tet–), the most abundant LSU product detected is the 5.8 kb pre-rRNA followed by the 5.1, 3.9 and 0.7 kb precursors. These pre-rRNAs, along with the 4.7, 3.3^a and 2.7 kb precursors show higher while the 5.4^{ab}, 5.0, 4.3^{ab} and 3.3^b kb show lower accumulation in TbRRP44 deficient cells (lanes Tet+).

(former 0.61 kb, as explained bellow) can also be detected in these cells at low levels (Figures 6D, 7 and 8). The 5.1 kb and 0.7 kb pre-rRNAs are generated by cleavage of the 5.8 kb LSU-B0 precursor in ITS2, at site C2. Similarly, low levels of the 4.4 kb (Figures 6C, 7C and D), 3.9 kb (Figures 6C, 7B, C), 0.65 kb (Figure 8E) and 0.2 kb (8E–G) precursors are also observed in control cells. Otherwise, all other processing sites seem to be simultaneously processed very quickly in control cells.

TbRRP44 deficiency caused a striking series of alterations in LSU pre-rRNA processing affecting the abundance of the pre-rRNAs that are detected in control cells with accumulation of the 5.8 kb LSU-B0/5.7 LSU-B1, 5.1, 3.9 and 0.7 kb pre-rRNAs, and decrease in the levels of the 4.4 and 0.2 kb pre-rRNAs in parallel with appearance of a variety of aberrant precursors that are not detected in control cells (Figures 6–8 'Tet +' lanes). The aberrant precur-

sors detected at higher levels include the 4.7 and 1.0 kb pre-rRNAs (Figures 6, 7 and 8E), and the 2.7 kb and 3.3^a kb pre-rRNAs (Figures 6 and 7). The 4.7 kb/B0-F1 and 1.0 kb/F1-3′-end pre-rRNAs are complementary segments that could be generated by cleavage of the 5.7 kb LSU-B0 pre-rRNA at site F1. Considering that the 1.0 kb pre-RNA is detected only by probe ITS7, its exact 5′ and 3′ boundaries were not determined in this work. That it comprises the segment containing SR2, SR6 and SR4 was tentatively deduced from the structure of pre-rRNA. The 2.7 kb/B0-D1 and 3.3^a kb/D1-3′-end pre-rRNAs are complementary segments that can be generated by cleavage of the 5.8 kb LSU-B0 pre-rRNA at site D1. The 2.7 kb/B0-D1 pre-rRNA is not detected by probe ITS3 (Figure 6C), indicating that site D1 is located nearby the 3′ end of the LSUα rRNA.

A second 3.3 kb pre-rRNA, named 3.3^b kb, is detected by the probes ITS2-b, ITS2-c and ITS2-d (right panel in
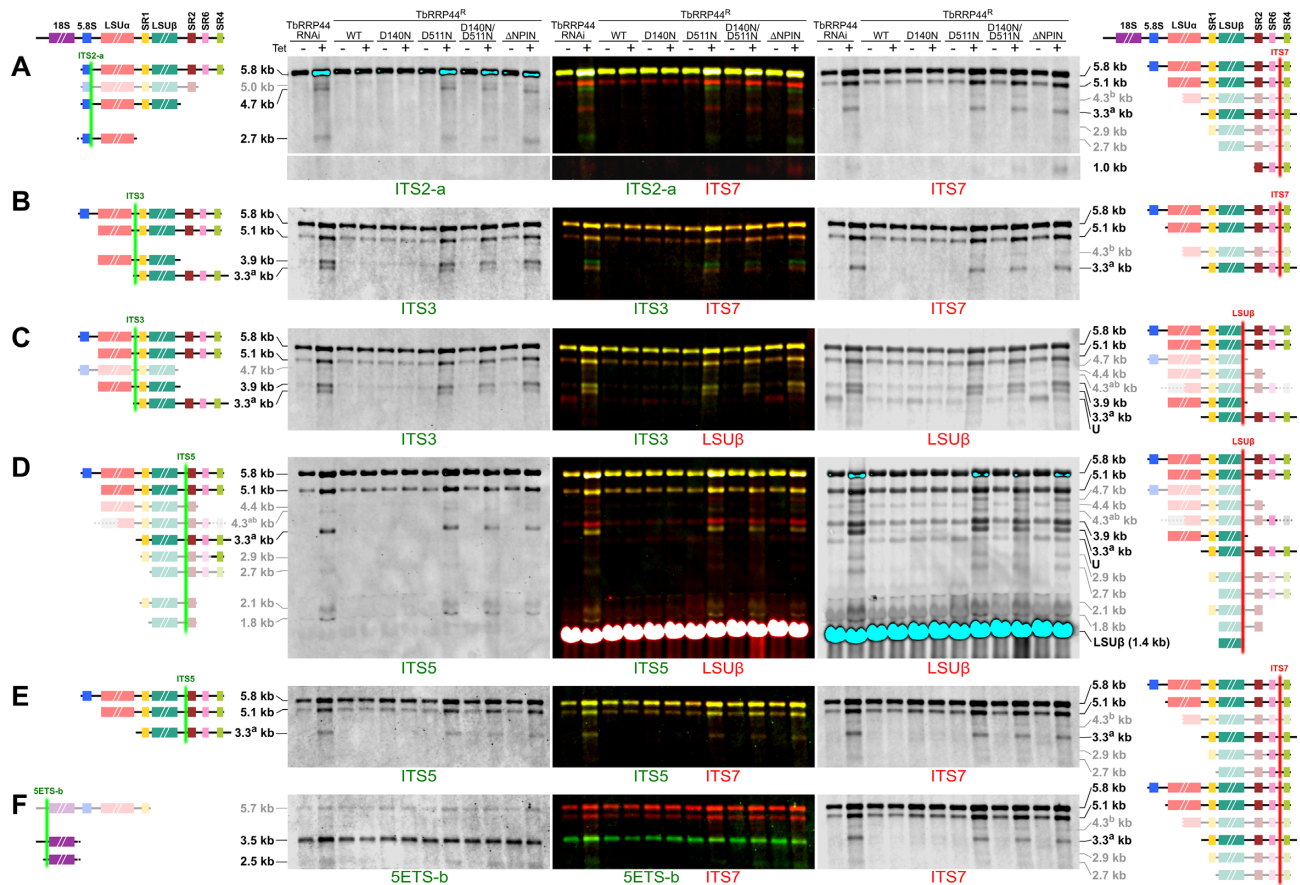
Figure 7. Analysis of LSU precursors by Northern blots with probes hybridizing in ITS3, LSUβ, ITS5 and ITS7. Northern blots with probes ITS2-a and 5ETS-b are also shown for comparison. Diagrams of the parts that compose each pre-rRNA fragment detected by each probe are indicated at the left and right sides of the images. The precursors detected at lower levels are indicated in fainter colors. The diagrams of the precursor 4.3^{ab} kb for which the 5′ and 3′ boundaries could not be assigned are marked in grey. Green and red vertical lines on the diagrams indicate the relative position of the probes on each pre-rRNA intermediate. In the Northern blot images, probes are identified at the bottom and the strains at the top of each panel, respectively. Tet - and + indicate, respectively, the cultures uninduced and induced with tetracycline. The central panels show overlays of the two respective Northern blots shown at left and right. Green bands indicate the precursors that are detected only by the probes of the left panels, red on the right panels, and orange/yellow indicates the precursors detected by both probes. (**A**) Northern blots performed with probes ITS2-a (left) and ITS7 (right). (**B**) Northern blots performed with probes ITS3 (left) and ITS7 (right). (**C**) Northern blots performed with probes ITS3 (left) and LSUβ (right) (images excluding the region of the mature LSUβ). (**D**) Northern blots performed with probes ITS5 (left) and LSUβ (right) (images including the region of the mature LSUβ). (**E**) Northern blots performed with probes ITS5 (left) and ITS7 (right). (**F**) Northern blots performed with probes 5ETS-b (left) and ITS7 (right). A series of precursors accumulate in the parental KD cells and in cells expressing non-complementing TbRRP44 mutants.

6B and C, both panels in 6D) but not by probes 5.8S and ITS2-a (Figure 6A, B). This indicates that its 5′-end must be generated by a cleavage in ITS2 between probes ITS2-a and ITS2-b. This cleavage site has not been described previously. In this work, it was tentatively termed cleavage site C1 to differentiate it from the site identified as C in some reports (45,46), which is located near the 5′-end of the LSUα in a position analogous to site C2 of the *S. cerevisiae* pre-rRNA. With the 5′-end starting at site C1, the 3′-end of the 3.3^b kb pre-rRNA would lie in the middle of the LSUβ, where another irregular cleavage should take place in TbRRP44-deficient cells.

Probe LSUβ was designed also with the intent of confirming the 3′-end of the LSUβ rRNA. Some sequences deposited in the databases report LSUβ rRNAs having a shorter 3′ region with 1484 nucleotides. Our data show that probe LSUβ hybridizes inside the mature LSUβ rRNA (Figure 7D). Its 3′-end is consistent with the results de-

scribed by White and co-workers (4), with 1536 nucleotides as the TriTrypDB tmp.1.60 sequence. Possibly due to a higher sensitivity, probes LSUβ and ITS5 revealed additional bands of the LSU maturation pathway. Both probes revealed additional pre-rRNAs with approximate sizes of 4.4 (5′-LSUα-G1), 2.9 (SR1-SR4), 2.7 (E1-SR4), 2.1 (D1-G1) and 1.8 (E1-SR2) kb pre-rRNAs containing the LSUβ and adjacent SR segments (Figure 7D). Probe LSUβ detected another band migrating between the 2.9 and 3.3^a kb precursors (labelled as 'U' for unknown in Figure 7C and D, right panels) that is not detected by probe ITS5. We could not assign any precursor to this band and assumed that it might result from an unspecific hybridization.

Among the large molecular mass precursors identified at low levels in TbRRP44-deficient cells are the 5.4, 5.0 and 4.3 kb pre-rRNAs (Figures 6 and 7). Assuming that processing occurs preferentially at the regular cleavage sites, the 5.0 kb pre-rRNA boundaries can be delimited to sites B1
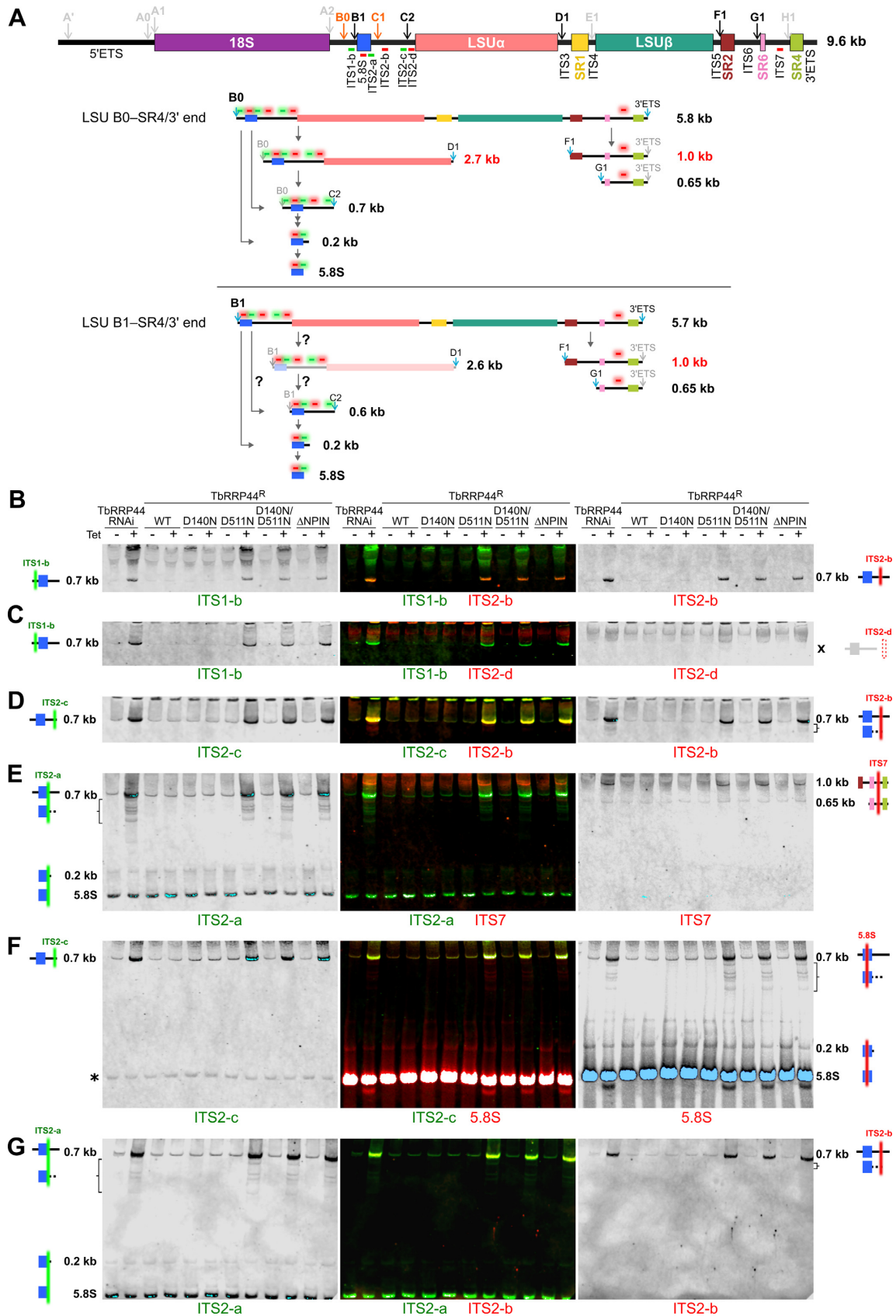
Figure 8. Analysis of small pre-rRNA fragments by northern blot. (**A**) Diagram of the *T. brucei* full-length pre-rRNA and tentative pre-rRNAs processing steps of the LSU-B0 and LSU-B1 pre-rRNAs leading to formation of the 5.8S rRNA and small LSU rRNAs from the 3′ region. Positions of the cleavage

and G1, including from the 5.8S rRNA up to SR2 (Figure 6, probes 5.8S, ITS2-a, ITS2-b and ITS2-c). In hybridizations with probes ITS2-d, ITS3, LSUβ and ITS5 the bands of the 5.0 kb and 5.1 kb pre-rRNAs would overlap (Figure 7B-E). The 5′ and 3′ boundaries of the 5.4 and 4.3 kb pre-rRNAs could not be differentiated with the probes used in this work and they should contain more than one species. They are identified as 5.4^a kb (B1-H1), 5.4^{ab} kb (B1-H1/C1-3′-end), 5.4^b kb (C1-3′-end); and 4.3^a kb (C1-F1), 4.3^{ab} kb (C1-F1/middle LSUα-SR4), 4.3^b kb (middle LSUα-SR4). Interestingly, the 4.3^b kb (middle LSUα-SR4) identified in this work may correspond to the aberrant pre-rRNA identified in previous studies as 3.8 kb* ([81]) and 4.5 kb* ([87]), which extends from the 3′-end up the middle of LSUα.

Similarly, a ~0.65 kb pre-RNA detected by probe ITS7 can be fitted to the segment from site G1 up to the 3′-end, but as in the case of the 1.0 kb, without additional probes it is not possible to conclusively describe its 5′ and 3′ boundaries (Figure 8E).

As described in previous studies ([58,64]), TbRRP44 knockdown leads to the accumulation of the 0.7 kb pre-rRNA and of a ladder of shorter intermediates containing the 5.8S rRNA with 3′ extensions of different lengths (Figure 8E–G). The 0.7 kb/B0-C2 pre-rRNA is detected by probes ITS1-b, 5.8S, ITS2-a, ITS2-b and ITS2-c, but not by probe ITS2-d, consistent with major cleavage sites between probes ITS1-a/ITS1-b and ITS2-c/ITS2-d (Figure 8). Hence, the size was redefined to contain at least 0.7 kb to include ITS2-c probe region, but size precision would depend on the exact location of the C2 cleavage site. Cleavage of the LSU-B1 pre-rRNA at site C2 would generate a ~0.6 kb/B1-C2 pre-rRNA. The polyacrylamide-urea gels used to analyze the small pre-rRNAs by Northern blot have resolution to separate the 0.7 kb/B0-C2 from the 0.6 kb/B1-C2 pre-rRNAs. The 0.7 kb/B0-C2 pre-rRNA can be unequivocally identified by probe ITS1-b (Figure 8B). However, the 0.6 kb/B1-C2 pre-rRNA would be mixed up with the shorter intermediates containing the 5.8S rRNA with 3′ extensions that are detected by probes 5.8S and ITS2-a. If present, the 0.6 kb/B1-C2 pre-rRNA would be detected also by probe ITS2-c, but a discrete band of 0.6 kb was not observed in the Northern blots with this probe (Figure 8). These results indicate that the LSU-B0 and LSU-B1 may not be equally processed at site C2.

A weak 0.2 kb pre-rRNA is detected by probes 5.8S and ITS2-a, but not by probes ITS1-b (upstream) and ITS2-b (downstream) (Figure 8), further indicating that it might originate from a cleavage at site between probes ITS2-a and ITS2-b. Such a 0.2 kb/B1-C1 pre-rRNA could originate from direct cleavage of the LSU-B1 pre-rRNA at site C1 (Figure 8A). Although it is detected at low levels, the images in Figure 8E (left panel) and 8F (right panel) indicate that there might be some reduction of the 0.2 kb pre-rRNA in TbRRP44 deficient cells. This could be caused both by accumulation of upstream precursors with partial 3′ processing or by slower processing of sites B1 and C1 in the larger precursors. In TbRRP44-deficient cells, a band smaller than the mature 5.8S rRNA is also detected by probe 5.8S, that might originate from aberrant processing or by partial degradation of the 5.8S rRNA (Figure 8F).

The pattern of precursors identified in different Northern blot hybridizations by probes that can detect the same pre-rRNA intermediates was quite reproducible. This led us to quantitatively estimate the relative amount of the different LSU rRNA intermediates that accumulate in TbRRP44-deficient cells (Supplementary Figure S3). Despite the high variation between the replicates, it was possible to observe some patterns. The larger LSU pre-rRNAs (5.8, 5.1 and 5.0 kb) presented lower accumulation, the pre-rRNAs that are detected al low levels in the control cells show intermediate accumulation (3.9 and 0.7 kb) and the ones that are detected only in TbRRP44 cells, both at higher (4.7, 3.3^a and 2.7 kb) and lower (4.3^b, 3.3^b kb) levels show higher accumulation (Supplementary Figure S3).

Effect of TbRRP44 deficiency on snoRNA and spliced leader processing

Homologues of TbRRP44 are known to play a general role in RNA metabolism by participating in the processing of RNA precursors transcribed by all three RNA polymerases. To investigate the effect of TbRRP44 deficiency on the processing of RNAs transcribed by RNA polymerase III we have selected three snoRNAs that have already been implicated in rRNA processing in *T. brucei*, including the U3 snoRNA, which is involved in processing of sites A0 and A1 of the SSU pre-rRNA ([85,88]), and the Tb9Cs3C3 and Tb10Cs4C3 snoRNAs that are involved in covalent modification and processing of the LSU pre-rRNA ([46,82]).

---

sites are indicated above the pre-rRNA diagram. Green and red boxes indicate the relative position of the probes on each pre-rRNA intermediate. The 5.8 kb LSU-B0 precursor and the unusual 2.7 kb precursor cleaved at sites B0 and D1 can give rise to the 0.7 kb pre-rRNA following a cleavage at site C2. A 0.2 kb pre-rRNA could be formed either by 5′-3′ or 3′-5′ processing of the 0.7 kb pre-rRNA or by direct cleavages of the 5.8 kb, 2.7 kb and 0.7 kb pre-rRNAs at sites B1 and C1. Processing of the 5.7 kb LSU-B1 would follow a similar pathway. However, the 0.6 kb and 2.6 kb pre-rRNA (processing steps indicated by question marks) were not unequivocally detected in this work. Precursors identified in red were only detected in TbRRP44 deficient cells. (**B**) Northern blots performed with probes ITS1-b (left) and ITS2-b (right). (**C**) Northern blots performed with probes ITS1-b (left) and ITS2-d (right). (**D**) Northern blots performed with probes ITS2-c (left) and ITS2-b (right). (**E**) Northern blots performed with probes ITS2-a (left) and ITS7 (right). (**F**) Northern blots performed with probes ITS2-c (left) and 5.8S (right). The asterisk indicates an unspecific hybridization. (**G**) Northern blots performed with probes ITS2-a (left) and ITS2-b (right). Central panels in B-G show overlays of the two respective Northern blots shown at left and right. Green bands indicate the precursors detected only by the probes of the left panels, red bands the precursors detected only by the probes of the right panels, and orange/yellow the precursors detected by both probes. Probes are identified at the bottom and the strains at the top of each panel, respectively. Brackets in E–G indicate the shorter products generated by incomplete processing of the 0.7 kb 3′-end and possibly also a 0.6 kb pre-rRNA. Diagrams of the parts that compose each pre-rRNA fragment detected are shown at the left and right sides of the images. Cultures uninduced and induced with tetracycline (Tet) are indicated by - and +, respectively. These analyses detected accumulation of the 0.7 kb pre-rRNA and of shorter processing products of the 0.7 kb pre-rRNA from the pathway leading to maturation of the 5.8S rRNA. Probe ITS2-b does not detect the 0.2 kb precursor supporting presence of a cleavage site between probes ITS2-a and ITS2-b. In addition, accumulation of a 1.0 kb pre-rRNA and of a 0.65 kb pre-rRNA is also detected comprising, the whole or part of the segment containing srRNAs 2, 6 and 4.
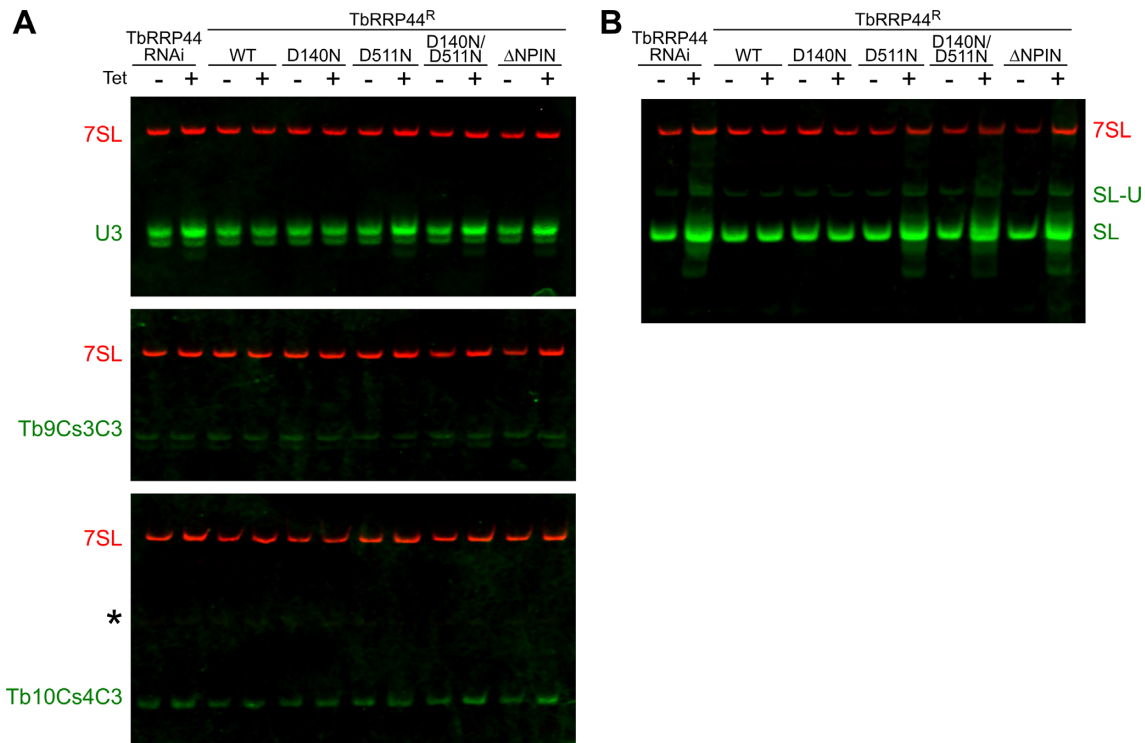
Figure 9. Effect of TbRRP44 knockdown on snoRNAs and spliced leader synthesis. The strains are identified at the top of each panel. – and + indicate the samples from cultures uninduced and induced with tetracycline (Tet). Each blot was co-hybridized with a signal recognition particle RNA probe (7SL). The Northern blot with the probes to detect the U3 snoRNA and the spliced leader were performed with 3 µg of total RNA, while the blots for the snoRNAs Tb9Cs3C3 and Tb10Cs4C3 were performed with 6 µg of total RNA. (**A**) Analysis of snoRNA synthesis. The probes used in the Northern blots of the respective snoRNAs are identified on the left side. In control cells, two bands were detected for the U3 snoRNA. In TbRRP44 deficient cells, there is accumulation of the larger band and presence of a shorter product, which should correspond respectively to U3 precursor and to a product of degradation or misprocessing of the U3 snoRNA. Two bands are also detected for the snoRNA Tb9Cs3C3 and a single band for the snoRNA Tb10Cs4C3. * Indicates an unspecific hybridization. No clear difference was observed for the snoRNAs Tb9Cs3C3 and Tb10Cs4C3 between control and TbRRP44 deficient cells. (**B**) Analysis of spliced leader synthesis. A major band corresponding to the mature spliced leader (SL) and a secondary band corresponding to 3′ poly-uridine extended products (SL-U) are detected in control cells (Tet–). In TbRRP44 deficient cells (Tet+) new larger and truncated forms of the spliced leader are observed.

Northern analyses revealed two bands for the U3 snoRNA in control cells. Even though several publications have reported a single band for *T. brucei* U3, considering that the hybridization pattern was reproducible, and that a recent publication has shown two bands for this snoRNA (89) we, therefore, assumed that the larger band corresponds to a precursor and the shortest one to the mature U3. In TbRRP44 deficient cells, there is accumulation of the larger band and appearance of a shorter product that may result from degradation or misprocessing of the U3 snoRNA (Figure 9A). Tb9Cs3C3 and Tb10Cs4C3 are less abundant and were not detected using the same amount of RNA loaded in the gels for analysis of the U3 snoRNA. Better results were obtained after increasing the amount of RNA for the Northern blots, but still they were at the limit of detection by the probes used in this work (Figure 9A). Nevertheless, two bands are also detected for the snoRNA Tb9Cs3C3 and a single band for the snoRNA Tb10Cs4C3. No clear difference was observed for these snoRNAs between control and TbRRP44 deficient cells (Figure 9A).

To test if TbRRP44 depletion also affects maturation of RNAs transcribed by RNA polymerase II, Northern blots were preformed to analyze the steady state of the spliced leader. A major and a secondary band of larger size are de-

tected in control cells (Figure 9B). According to previous studies, the major band corresponds to the mature spliced leader, and the secondary band of larger size corresponds to 3′ poly-uridine extended products (90–94). Interestingly, TbRRP44 deficiency led to the appearance of both larger and truncated forms of the spliced leader, which are phenotypes similar with those already described for depletion of the SNIP 3′-5′ exonuclease (92), exportin 1 (90), SmE and SmD1 (91,93) and the La protein (94). Our results confirm the requirement of TbRRP44 for accurate processing of the spliced leader and, together with the alterations in processing of U3 in TbRRP44 deficient cells, show that TbRRP44 may have a wide role in RNA processing in *T. brucei*.

DISCUSSION

Genetic complementation of TbRRP44 knockdown using RNAi-resistant variants

In this study, we employed a combined genetic system, which allows for simultaneous knockdown of the endogenous TbRRP44 protein and parallel induction of TbRRP44 RNAi-resistant variants for evaluation of their complementation efficiency. One component of the genetic system contains the T7 RNA polymerase, T7 RNA promoters and

the tetracycline repressor/Tet operator pair for knockdown the endogenous TbRRP44 protein and, the other, contains a ribosomal RNA intergenic region with the tetracycline repressor/Tet operator pair for regulated expression of the complementing proteins to be tested (64,71,72). This complementation system led to overexpression of the RNAi-resistant variants. However, since complementation with the wild type TbRRP44 did not cause any phenotype associated either to overexpression or to the presence of the HA-tag, it was considered suitable for the functional analysis of TbRRP44 variants.

Requirement of TbRRP44 for cell growth and some steps of pre-rRNA processing has been demonstrated in previous studies using RNAi-induced knockdown of the wild-type protein (58,64). The strategy used in this work allowed us to investigate the requirement of each catalytic domain of TbRRP44 for pre-rRNA processing. Interestingly, the TbRRP44$^{R-D511N}$ variant, containing the D511N mutation that inactivates the exonucleolytic site, was not able to complement the knockdown of the endogenous TbRRP44, showing that the exonuclease activity is essential for TbRRP44 function. This finding contrasts with the phenotypes described for *S. cerevisiae*. Despite causing strong phenotypes in growth and pre-rRNA processing, *S. cerevisiae* RRP44 exonucleolytic site mutants are still viable (50,52–54).

Contrary to the D511N mutation, knockdown of the endogenous TbRRP44 protein was fully complemented by the TbRRP44$^{R-D140N}$ variant containing the D140N mutation, which is expected to abolish the activity of the endonucleolytic domain (64). This result is not surprising since mutations in the catalytic site of the *S. cerevisiae* and human RRP44 PIN domain also did not lead to detectable phenotypes (50,52,53,57). However, deletion of the N-terminal and PIN domain (TbRRP44^{R}-ΔNPIN) prevented complementation of the endogenous TbRRP44 knockdown, showing that the physical presence of the PIN domain itself is required for TbRRP44 protein function. This finding indicates a conservation of the PIN and RNB domain functional interdependence as observed for the *S. cerevisiae* and human RRP44 counterparts (50,52–54,57,95). The double mutant variant TbRRP44$^{R-D140N/D511N}$ is not able to complement the knockdown of the endogenous TbRRP44 and its phenotypes overlaps with the ones shown by the exonucleolytic site single mutant and the PIN domain deletion mutant.

The PIN domain of the *S. cerevisiae* and human RRP44 proteins contributes for the exonuclease activity possibly by playing a role both in interaction with the exosome (61–63) and with RNA substrates (53,96). In the case of *T. brucei*, the evidence available so far indicates that TbRRP44 does not associate stably to the exosome complex (58–60). Therefore, we can hypothesize that the PIN domain cooperates with the exonucleolytic activity of the RNB domain most probably by mediating interaction with RNA substrates. Consistently, RNA binding assays performed in a parallel study provided evidence for the role of the PIN domain of TbRRP44 (Cesaro *et al.*, 2022, manuscript submitted in parallel to *NAR*). Interaction assays performed with the catalytically inactive full-length TbRRP44$^{D140N/D511N}$ and TbRRP44-ΔNPIN^{D511N}

proteins showed that the TbRRP44-ΔNPIN^{D511N} protein interacts less efficiently with structured RNA lacking a 3′ overhang. In addition, the interaction of TbRRP44 with unstructured and structured RNAs with and without a 3′overhang follows the Hill model of positive cooperativity, further supporting the cooperative function of the PIN domain.

Early ITS1 cleavages separating the SSU from the LSU precursor and identification of a second endonucleolytic cleavage site in ITS1

Concerning pre-rRNA processing defects, the strains carrying the TbRRP44$^{R-D511N}$, TbRRP44$^{R-D140N/D511N}$ and TbRRP44^{R}-ΔNPIN variants and the parental conditional strain showed similar results for all pre-rRNA segments analyzed by Northern blots. The only noticeable difference is related to the 3.5 kb SSU precursor that seems to accumulate at a higher amount in the TbRRP44 parental knockdown strain as compared to the strains carrying the TbRRP44$^{R-D511N}$, TbRRP44$^{R-D140N/D511N}$ and TbRRP44^{R}-ΔNPIN variants (Figure 4E, F). Although there are no detectable phenotypic differences between these variants, the extensive analysis performed in this work revealed the requirement of TbRRP44 for processing of a series of pre-rRNA intermediates and provided new insights into the complex pathway of pre-rRNA maturation in *T. brucei*.

The low amount detected for the 9.6 kb primary precursor is consistent with previous reports showing that it is quickly converted into two fragments, termed SSU and LSU precursors, with sizes ranging from 3.4 to 3.5 kb for the SSU and 5.7–5.8 kb for the LSU (45,82). Previous studies have assumed that a single cleavage separates the SSU and LSU precursors, taking place at site B1, located in ITS1 near the 5′-end of the 5.8S rRNA (46,81,83,84,97). However, thanks to the position of probe ITS1-b used in this work, we found that approximately half of the SSU and LSU precursors can be generated sharing a common sequence of ITS1, comprising the segment recognized by probe ITS1-b. This can only be possible if two non-simultaneous endonucleolytic cleavages take place in ITS1. Since the second site is located upstream the previously known site B1, the new site was tentatively named 'B0' in this work. Some studies may have missed the second cleavage site by using only probes located in ITS1 upstream of the site B0 (46,98). The newly identified endonucleolytic cleavage site (B0) was mapped between the nucleotides -136/137 upstream to the 5′-end of the mature 5.8S rRNA.

The finding that two non-simultaneous endonucleolytic cleavages take place in ITS1 is not exclusive from *T. brucei*. This has already been reported for processing of mice ITS1 (79), which can be processed at sites 2b and 2c. Actually, two endonucleolytic cleavage sites have been identified in ITS1 of all eukaryotes, although they not always lead to productive rRNA maturation. In *S. cerevisiae*, under normal physiological conditions, a major pathway proceeds through cleavage at site A2, located at a proximal position as *T. brucei* site B0. A switch to cleavage at site A3 takes place under nutritional and stress conditions leading both SSU and LSU precursors to degradation (99,100), appar-

ently as part of regulated cellular responses (101). In plants and human cells, both sites can be utilized for productive rRNA maturation, although there is a preference for the distal site (A3 in plants and 2 in human cells; reviewed in Tomecki *et al.* (47)). Preference for the distal site (site 2c) was also observed for mice tissues, although mouse-derived NIH 3T3 cells show processing at comparable rates for both proximal (2b) and distal ITS1 endonucleolytic cleavage sites (79). In *T. brucei* control cells, the ratio of LSU/SSU precursors detected by probe ITS1-b indicates that both sites are cleaved at similar rates. In cells expressing the non-complementing TbRRP44[R-D511N], TbRRP44[R-D140N/D511N] and TbRRP44[R]-ΔNPIN mutants, this ratio increases, indicating either a shift in the cleavage of ITS1 from site B1 to site B0 or an accumulation of the LSU precursor cleaved at site B0 (Figure 4F). As a result of two non-simultaneous endonucleolytic cleavages in ITS1, two SSU precursors with different 3′-ends are generated, one between probes ITS1-a and ITS1-b (SSU-B0, 3.4 kb) and another between probe ITS1-b and the 5′-end of the 5.8S rRNA (SSU-B1, 3.5 kb). Consequently, two LSU precursors are also generated with different 5′-ends (LSU-B0, 5.8 kb, and LSU-B1, 5.7 kb) (Figures 4 and 10).

Requirement of TbRRP44 for degradation of the excised 5′ETS and processing of the ITS1 segment of the SSU pre-rRNA

There is an indication from the work by Hartshorne and Toyofuku (85) that the short 5′-ETS segment from the 5′-end to site A′ is removed by an early cleavage. The A′ cleavage has also been proposed to precede all downstream processing events (88). Processing at sites A0 and A1 of both SSU precursors (SSU-B0 and SSU-B1) is dependent on the U3 snoRNA (85,88). The excised 5′-ETS fragment accumulates in TbRRP44 knockdown cells and in cells expressing functionally deficient TbRRP44 mutants. Similar requirement for degradation of the excised 5′-ETS has been reported for the human, yeast, and plant cells RRP44 homologues. Our finding shows that the mechanism of degradation of the excised 5′-ETS is conserved in all eukaryotes (57,102,103).

Considering the positions of probes ITS1-a and ITS1-b and of the B0 and B1 sites, processing of the 3.4–3.5 kb SSU pre-RNAs at sites A0 and A1 gives rise to 2.5–2.6 kb SSU fragments with at least 201 and 263 nucleotides, respectively, at the 3′-end. A 2.6 kb precursor equivalent to the ones detected in this work has been previously reported in control cells by Faktorová and co-workers (84), who showed that TbUTP10 is involved in the early stages of 18S rRNA synthesis. In conditions of TbRRP44 deficiency, the 2.5/2.6 kb precursor shows a high intensity signal, at a ratio nearly 1:1 with the 3.5 kb SSU precursor. Accumulation of these 2.5–2.6 kb SSU intermediates reveals that the cleavages at sites A0 and A1 occur before processing of the ITS1 segment of the SSU pre-rRNA. In addition, probe 5ETS-b can differentially detect a ∼2.5 kb species containing the A0-A1 segment. Accumulation of 2.5 kb SSU pre-rRNAs containing the A0-A1 segment indicates that there should be slower processing or accumulation of the ∼2.5 kb species extending up to site A0. Accumulation of these 2.5–2.6 kb

SSU intermediates implicate TbRRP44 in the removal of the ITS1 region starting at B1 and B0 towards the 3′-end of the 18S rRNA. After removal of the region comprising probe ITS1-a, most probably the 3′-to-5′ degradation stops at some point downstream the 3′ and, the last segment is excised latter by an endonucleolytic cleavage at site A2 mediated by NOB1/PNO1 (83).

The requirement of TbRRP44 for removal of the proximal part of ITS1 during maturation of the 18S rRNA 3′-end resembles the mechanism used by human and plant cells which, after an initial endonucleolytic cleavage, involves 3′-5′ exonucleolytic trimming. However, both in human and plant cells this 3′-5′ processing of ITS1 has been attributed to the exosome complex with evidence indicating the RRP6 homologues play a major role in this process (104–106).

Although the exact position of site B1 has not been precisely mapped yet, evidence obtained with *T. brucei* cells deficient for the 5′-3′ exonuclease XRNE (86) indicates that it should be located near the 5′-end of the 5.8S rRNA. XRNE-deficient cells accumulate a 5.8S rRNA with a short extension at the 5′-end, which most probably coincides with the position of the B1 cleavage site. The sequence spanning downstream from the 3′ of probe ITS1-b up to the 5′-end of the 5.8S rRNA is only 68 nucleotides long. Therefore, our results are also consistent with a cleavage near the 5′-end of the 5.8S rRNA, corresponding to site B1.

LSU pre-rRNA processing defects in TbRRP44 deficient cells

TbRRP44 deficiency resulted in accumulation of a large number of LSU pre-rRNAs, some showing higher and others lower abundance. Among the group that accumulates at higher levels are the 5.7/5.8 kb, 5.1 kb, 0.7 kb and 3.9 kb pre-rRNAs, which were detected both in control and TbRRP44 deficient cells. The group of precursors accumulating at higher levels in TbRRP44 deficient cells includes also the 4.7 and 1.0 kb pre-rRNAs and the 2.7 kb and 3.3[a] kb pre-rRNAs that were detected only in TbRRP44 deficient cells. As described in the results section and summarized in Figure 10, for these pre-rRNAs, the Northern analyses allowed for a relatively consistent definition of their 5′ and 3′ boundaries. For a set of low level pre-rRNAs including the 5.0 and 4.4 kb pre-rRNAs and those detected by probes LSUβ and ITS5, it was also possible to tentatively propose defined 5′ and 3′ boundaries. However, for others identified as 3.3[b], 4.3[a], 4.3[b], 4.3[ab], 5.4[a], 5.4[b] and 5.4[ab] kb it was not possible to propose specific 5′ and 3′ boundaries.

In *T. brucei*, accumulation of a set of LSU intermediates was observed for the conditional depletion of the ribosomal protein L5 (107), the non-conserved phosphoprotein NOPP44/46 (87), the NOG1 homolog (108) and the splicing factor homologs TSR1, TSR1IP and U2AF35 (109). However, none of these proteins possess intrinsic catalytic activity. In the case of TbRRP44, in addition to accumulation of the 0.7 kb precursor, which is a marker for TbRRP44 deficiency in all organisms tested, TbRRP44 deficiency resulted in slow processing of all ITSs of the LSU precursor. This indicates that after the initial endonucleolytic cleavages, TbRRP44 may have a general role in the 3′-to-5′ ex-
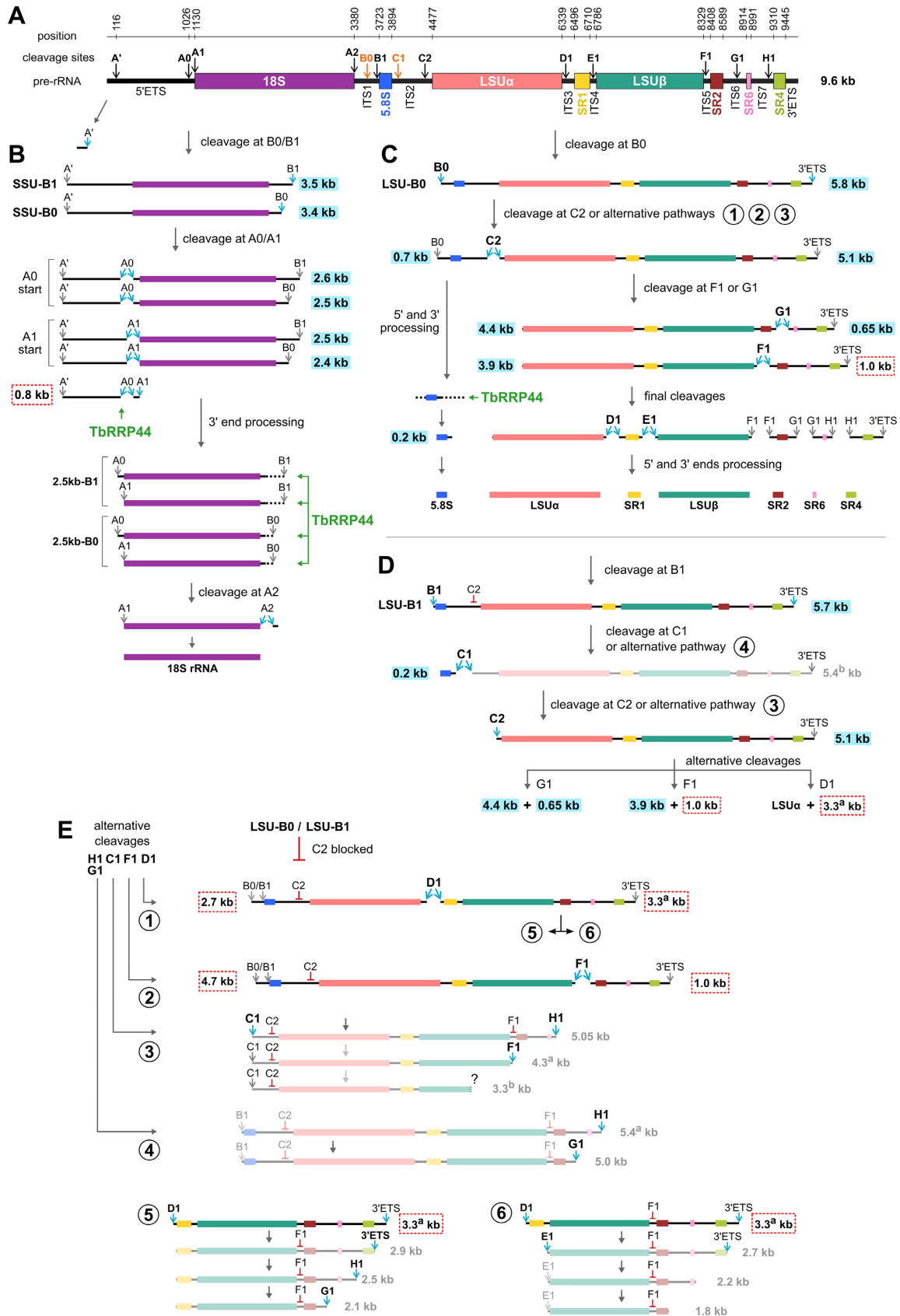
Figure 10. Overview of the pre-rRNA processing pathway in TbRRP44 deficient cells. (**A**) Diagram of *T. brucei* pre-rRNA structure with the positions of the cleavage sites. (**B**) Pre-rRNA intermediates of the SSU pathway. The 9.6 kb pre-rRNA is initially processed either at site B0 or B1 in ITS1 producing two

onucleolytic removal of the ITS segments of the LSU intermediate precursors.

Involvement of TbRRP44 in snoRNA U3 and spliced leader processing

In *T. brucei*, the general accumulation of rRNA precursors observed in cells with knockdown or functional deficiency of TbRRP44 has some parallel with the knockdown of TbNOP1, the catalytic subunit of the box C/D snoRNP complex responsible for rRNA methylation [81]. TbNOP1-depleted cells also showed accumulation of the 3.5 kb and 2.6 kb SSU precursors as well as the 5.8, 5.1, 3.9, 2.7 kb LSU precursors [81]. As described previously, several snoRNAs participate in pre-rRNA processing in *T. brucei* [46,82,85,88]. While depletion of the U3 affects processing of the 5′ ETS of the SSU precursors [85,88], Chikne and co-workers [46] described a set of snoRNAs whose depletion leads to accumulation of pre-rRNAs especially of the LSU pathway. In this work, we demonstrated that processing of the U3 snoRNA is affected by TbRRP4 depletion. Despite this defect, just a subtle increase of the 3.5 kb SSU-B1 precursor was observed in TbRRP44 deficient cells (Figure 4E, graph on the right). This indicates that even though depletion of TbRRP44 can indirectly affect pre-rRNA processing, in this case the effect was minimal. However, the requirement of TbRRP44 for processing of the spliced leader may affect the synthesis of other protein factors involved in pre-rRNA processing, adding up to the secondary effects that take place in pre-rRNA processing in parallel with the primary defects caused by TbRRP44 depletion.

Concluding remarks

As reported in previous studies [58,64], slow processing of the 3′-end of the 0.7 kb precursor can be explained as a direct effect of TbRRP44 deficiency. Taking into account the conservation of the pre-RNA processing factors in eukaryotes, it is possible to consider that accumulation of the excised 5′-ETS segment and of the 2.5/2.6 kb SSU pre-rRNAs containing the 18S rRNA and the ITS1 segment up to sites B0 and B1 are also due to a direct effect of TbRRP44 deficiency. However, the pre-rRNA processing analysis described in this work does not demonstrate a direct role of TbRRP44 in the endonucleolytic cleavages of the LSU spacer sequences. One hypothesis can be proposed considering that, as in the case of the excised 5′-ETS, ITS1 and ITS2, the action of TbRRP44 on the other ITSs starts after a previous endonucleolytic cleavage carried out by a still unknown factor. In this context, slow endonucleolytic processing of the LSU spacer sequences would be due to feedback regulation caused by accumulation of unprocessed precursors after TbRRP44 depletion.

In summary, the results presented in this work illustrate the requirement of TbRRP44 for removal of transcribed spacer sequences and shed light onto the intricate mechanism of trypanosomatid pre-rRNA processing (Figure 10) and implicate TbRRP44 in processing of RNA precursors transcribed also by the RNA Polymerases II and III. A new endonucleolytic cleavage site in ITS1 was identified, which takes place in the initial pre-rRNA processing steps that separate the SSU from the LSU precursors. In addition to the maturation of the 5.8S rRNA 3′-end, we showed that TbRRP44 is required also for degradation of the excised 5′-ETS and for 3′-5′ removal of the ITS1, after the initial endonucleolytic cleavages. Our data indicate that, under normal conditions, processing of the ITSs of the 5.8 kb LSU precursor take place nearly simultaneously while TbRRP44 depletion reduces the processing rate causing accumulation of a series of intermediate LSU precursors.

DATA AVAILABILITY

All data are available in the main text or the Supplementary Data files.

SUPPLEMENTARY DATA

Supplementary Data are available at NAR Online.

SSU pre-rRNAs with different 3′-end, the longer identified as 3.5 kb (SSU-B1) and the shorter as 3.4 kb (SSU-B0). Subsequent non simultaneous cleavages of sites A0 and A1 liberate a 5′ ETS, producing up to four different species of the ~2.5 kb SSU pre-rRNAs (A0-B1, A1-B1, A0-B0 and A1-B0). Based on the conservation of pre-rRNA processing in eukaryotes, it is very likely that TbRRP44 participates directly in the removal of part of the ITS1 segment that remains in the 3′ of the SSU precursors, which are finally processed at site A2, generating the mature 18S rRNA. (**C**) Tentative processing pathway of the 5.8 kb LSU-B0 pre-rRNA. Following cleavage of the 9.6 kb pre-rRNA at site B0, the LSU-B0 seems to be initially processed at site C2 separating the 0.7 pre-rRNA of the 5.8 rRNA pathway from the 5.1 kb pre-rRNA containing the remaining LSU pre-rRNAs. The 5.1 kb pre-rRNA is processed at site G1 in ITS6 or at site F1 in ITS5, generating the 4.4 and 3.9 kb pre-rRNAs. These two cleavages of the 5.1 kb pre-rRNA generate complementary pre-rRNAs of 0.65 and 1.0 kb pre-rRNAs containing SR pre-rRNAs. The 3.9 kb pre-rRNA can also be produced by cleavage of the 4.4 kb pre-rRNA at site F1. Except for the 4.4 kb and 0.2 kb pre-rRNA that show decrease, all other LSU pre-rRNAs accumulate in TbRRP44 deficient cells. (**D**) Tentative processing pathway of the 5.7 kb LSU-B1 pre-rRNA. Following cleavage of the 9.6 kb pre-rRNA at site B1, the LSU-B1 could follow the same pathway of LSU-B0. An initial cleavage at site C2 would generate a 0.6 kb pre-rRNA that was not detected in our analyses. A small fraction is processed at site C1, producing the 0.2 kb and 5.4^b kb pre-rRNAs. A cleavage of both the LSU-B1 and the 5.4^b kb pre-rRNAs generates the 5.1 kb pre-rRNA whose processing can follow the same pathway as the 5.1 kb originating from processing of the LSU-B0 pre-rRNA at site C2. (**E**) Alternative pathways under TbRRP44 deficiency. Accumulation of the 5.8 kb (LSU-B0) allows for the LSU pre-rRNA to be processed either at site D1 in ITS3 (alternative pathway 1), or at site F1 in ITS5 (alternative pathway 2) before processing of site C2 in ITS2. These generates, respectively, the 2.7 and 3.3^a kb pre-rRNAs, and the 4.7 and 1.0 kb pre-rRNAs. Subsequent processing of the 3.3^a kb pre-rRNA follows the alternative pathways (5) and (6) below. Alternative pathway (3), starting from an LSU pre-rRNA comprising from site C1 to H1 (5.05 kb), describes the possible processing steps to generate the 4.3^a and 3.3^b kb pre-rRNAs. Alternative pathway (4) describes the possible steps for formation of the 5.0^b kb pre-rRNA starting from the 5.4^a kb pre-rRNA. Alternative pathways (5) and (6) describe the sequential processing steps in the maturation pathway of the LSUβ and SR pre-rRNAs starting from the 3.3^a kb pre-rRNA. Due to space limitations, not all possible alternative pathways can be represented. The pre-rRNA identifications on blue boxes indicate the pre-rRNAs detected in control cells that also accumulate in TbRRP44 deficient cells. Those in red boxes indicate the pre-rRNAs that accumulate at higher levels in TbRRP44 deficient cells only, and those in gray without boxes are the ones detected at low levels in TbRRP44 deficient cells only.

REFERENCES

1. Gray,M.W. (1979) The ribosomal RNA of the trypanosomatid protozoan *Crithidia fasciculata*: physical characteristics and methylated sequences. *Can. J. Biochem.*, **57**, 914–926.
2. Gray,M.W. (1981) Unusual pattern of ribonucleic acid components in the ribosome of *Crithidia fasciculata*, a trypanosomatid protozoan. *Mol. Cell. Biol.*, **1**, 347–357.
3. Spencer,D.F., Collings,J.C., Schnare,M.N. and Gray,M.W. (1987) Multiple spacer sequences in the nuclear large subunit ribosomal RNA gene of *Crithidia fasciculata*. *EMBO J.*, **6**, 1063–1071.
4. White,T.C., Rudenko,G. and Borst,P. (1986) Three small RNAs within the 10 kb trypanosome rRNA transcription unit are analogous to Domain VII of other eukaryotic 28S rRNAs. *Nucl Eic Acids Res.*, **14**, 9471–9489.
5. Campbell,D.A., Kubo,K., Clark,C.G. and Boothroyd,J.C. (1987) Precise identification of cleavage sites involved in the unusual processing of trypanosome ribosomal RNA. *J. Mol. Biol.*, **196**, 113–124.
6. Hernández,R., Díaz-de León,F. and Castañeda,M. (1988) Molecular cloning and partial characterization of ribosomal RNA genes from *Trypanosoma cruzi*. *Mol. Biochem. Parasitol.*, **27**, 275–279.
7. Torres-Machorro,A.L., Hernández,R., Cevallos,A.M. and López-Villaseñor,I. (2010) Ribosomal RNA genes in eukaryotic microorganisms: witnesses of phylogeny? *FEMS Microbiol. Rev.*, **34**, 59–86.
8. Hernández,R. and Cevallos,A.M. (2014) Ribosomal RNA gene transcription in trypanosomes. *Parasitol. Res.*, **113**, 2415–2424.
9. Schnare,M.N. and Gray,M.W. (1990) Sixteen discrete RNA components in the cytoplasmic ribosome of *Euglena gracilis*. *J. Mol. Biol.*, **215**, 73–83.
10. Schnare,M.N., Cook,J.R. and Gray,M.W. (1990) Fourteen internal transcribed spacers in the circular ribosomal DNA of *Euglena gracilis*. *J. Mol. Biol.*, **215**, 85–91.
11. Evguenieva-Hackenberg,E. (2005) Bacterial ribosomal RNA in pieces. *Mol. Microbiol.*, **57**, 318–325.
12. Boer,P.H. and Gray,M.W. (1988) Scrambled ribosomal RNA gene pieces in *Chlamydomonas reinhardtii* mitochondrial DNA. *Cell*, **55**, 399–411.
13. Milbury,C.A., Lee,J.C., Cannone,J.J., Gaffney,P.M. and Gutell,R.R. (2010) Fragmentation of the large subunit ribosomal RNA gene in oyster mitochondrial genomes. *BMC Genomics*, **11**, 485.
14. Spencer,D.F. and Gray,M.W. (2011) Ribosomal RNA genes in *Euglena gracilis* mitochondrial DNA: fragmented genes in a seemingly fragmented genome. *Mol. Genet. Genomics*, **285**, 19–31.
15. Feagin,J.E., Harrell,M.I., Lee,J.C., Coe,K.J., Sands,B.H., Cannone,J.J., Tami,G., Schnare,M.N. and Gutell,R.R. (2012) The fragmented mitochondrial ribosomal RNAs of *Plasmodium falciparum*. *PLoS One*, **7**, e38320.
16. Jackson,C.J., Gornik,S.G. and Waller,R.F. (2012) The mitochondrial genome and transcriptome of the basal dinoflagellate *Hematodinium* sp.: character evolution within the highly derived mitochondrial genomes of dinoflagellates. *Genome Biol. Evol.*, **4**, 59–72.
17. Kiethega,G.N., Yan,Y., Turcotte,M. and Burger,G. (2013) RNA-level unscrambling of fragmented genes in *Diplonema mitochondria*. *RNA Biol.*, **10**, 301–313.
18. Gray,M.W. (2014) Organelle evolution, fragmented rRNAs, and Carl. *RNA Biol.*, **11**, 213–216.
19. Jackson,S.A., Cannone,J.J., Lee,J.C., Gutell,R.R. and Woodson,S.A. (2002) Distribution of rRNA introns in the three-dimensional structure of the ribosome. *J. Mol. Biol.*, **323**, 35–52.
20. Dawid,I.B. and Rebbert,M.L. (1981) Nucleotide sequences at the boundaries between gene and insertion regions in the rDNA of *Drosophila melanogaster*. *Nucleic Acids Res.*, **9**, 5011–5020.
21. Roiha,H., Miller,J.R., Woods,L.C. and Glover,D.M. (1981) Arrangements and rearrangements of sequences flanking the two types of rDNA insertion in *D. melanogaster*. *Nature*, **290**, 749–753.
22. Woolford,J.L. and Baserga,S.J. (2013) Ribosome biogenesis in the yeast *Saccharomyces cerevisiae*. *Genetics*, **195**, 643–681.
23. Baßler,J. and Hurt,E. (2019) Eukaryotic ribosome assembly. *Annu. Rev. Biochem.*, **88**, 281–306.
24. Cheng,J., Lau,B., La Venuta,G., Ameismeier,M., Berninghausen,O., Hurt,E. and Beckmann,R. (2020) 90S pre-ribosome transformation into the primordial 40S subunit. *Science*, **369**, 1470–1476.
25. Du,Y., An,W., Zhu,X., Sun,Q., Qi,J. and Ye,K. (2020) Cryo-EM structure of 90S small ribosomal subunit precursors in transition states. *Science*, **369**, 1477–1481.
26. Lau,B., Cheng,J., Flemming,D., La Venuta,G., Berninghausen,O., Beckmann,R. and Hurt,E. (2021) Structure of the maturing 90S pre-ribosome in association with the RNA exosome. *Mol. Cell*, **81**, 293–303.
27. Heuer,A., Thomson,E., Schmidt,C., Berninghausen,O., Becker,T., Hurt,E. and Beckmann,R. (2017) Cryo-EM structure of a late pre-40S ribosomal subunit from *Saccharomyces cerevisiae*. *Elife*, **6**, e30189.
28. Scaiola,A., Peña,C., Weisser,M., Böhringer,D., Leibundgut,M., Klingauf-Nerurkar,P., Gerhardy,S., Panse,V.G. and Ban,N. (2018) Structure of a eukaryotic cytoplasmic pre-40S ribosomal subunit. *EMBO J.*, **37**, e98499.
29. Shayan,R., Rinaldi,D., Larburu,N., Plassart,L., Balor,S., Bouyssié,D., Lebaron,S., Marcoux,J., Gleizes,P.E. and Plisson-Chastang,C. (2020) Good vibrations: structural remodeling of maturing yeast pre-40s ribosomal particles followed by cryo-electron microscopy. *Molecules*, **25**, 1125.
30. Kater,L., Thoms,M., Barrio-Garcia,C., Cheng,J., Ismail,S., Ahmed,Y.L., Bange,G., Kressler,D., Berninghausen,O., Sinning,I. *et al.* (2017) Visualizing the assembly pathway of nucleolar pre-60S ribosomes. *Cell*, **171**, 1599–1610.
31. Biedka,S., Micic,J., Wilson,D., Brown,H., Diorio-toth,L. and Woolford,J.L. (2018) Hierarchical recruitment of ribosomal proteins and assembly factors remodels nucleolar pre-60s ribosomes. *J. Cell Biol.*, **217**, 2503–2518.
32. Sanghai,Z.A., Miller,L., Molloy,K.R., Barandun,J., Hunziker,M., Chaker-Margot,M., Wang,J., Chait,B.T. and Klinge,S. (2018) Modular assembly of the nucleolar pre-60S ribosomal subunit. *Nature*, **556**, 126–129.
33. Kiss-László,Z., Henry,Y., Bachellerie,J.P., Caizergues-Ferrer,M. and Kiss,T. (1996) Site-specific ribose methylation of preribosomal RNA: a novel function for small nucleolar RNAs. *Cell*, **85**, 1077–1088.
34. Ganot,P., Bortolin,M.L. and Kiss,T. (1997) Site-specific pseudouridine formation in preribosomal RNA is guided by small nucleolar RNAs. *Cell*, **89**, 799–809.
35. Ni,J., Tien,A.L. and Fournier,M.J. (1997) Small nucleolar RNAs direct site-specific synthesis of pseudouridine in ribosomal RNA. *Cell*, **89**, 565–573.
36. Reichow,S.L., Hamma,T., Ferré-D'Amaré,A.R. and Varani,G. (2007) The structure and function of small nucleolar ribonucleoproteins. *Nucleic Acids Res.*, **35**, 1452–1464.
37. Wild,T., Horvath,P., Wyler,E., Widmann,B., Badertscher,L., Zemp,I., Kozak,K., Csucs,G., Lund,E. and Kutay,U. (2010) A protein inventory of human ribosome biogenesis reveals an essential

function of exportin 5 in 60S subunit export. *PLoS Biol.*, **8**, e1000522.

38. Tafforeau,L., Zorbas,C., Langhendries,J.L., Mullineux,S.T., Stamatopoulou,V., Mullier,R., Wacheul,L. and Lafontaine,D.L.J. (2013) The complexity of human ribosome biogenesis revealed by systematic nucleolar screening of pre-rRNA processing factors. *Mol. Cell*, **51**, 539–551.

39. Badertscher,L., Wild,T., Montellese,C., Alexander,L.T., Bammert,L., Sarazova,M., Stebler,M., Csucs,G., Mayer,T.U., Zamboni,N. *et al.* (2015) Genome-wide RNAi screening identifies protein modules required for 40S subunit synthesis in Human cells. *Cell Rep.*, **13**, 2879–2891.

40. Farley-Barnes,K.I., McCann,K.L., Ogawa,L.M., Merkel,J., Surovtseva,Y.V. and Baserga,S.J. (2018) Diverse regulators of Human ribosome biogenesis discovered by changes in nucleolar number. *Cell Rep.*, **22**, 1923–1934.

41. Sharma,S., Marchand,V., Motorin,Y. and Lafontaine,D.L.J. (2017) Identification of sites of 2′-O-methylation vulnerability in human ribosomal RNAs by systematic mapping. *Sci. Rep.*, **7**, 11490.

42. Penzo,M. and Montanaro,L. (2018) Turning uridines around: role of rRNA pseudouridylation in ribosome biogenesis and ribosomal function. *Biomolecules*, **8**, 38.

43. Streit,D. and Schleiff,E. (2021) The *Arabidopsis* 2′-O-ribose-methylation and pseudouridylation landscape of rRNA in comparison to Human and yeast. *Front. Plant Sci.*, **12**, 684626.

44. Liang,X.H., Uliel,S., Hury,A., Barth,S., Doniger,T., Unger,R. and Michaeli,S. (2005) A genome-wide analysis of C/D and H/ACA-like small nucleolar rnas in *Trypanosoma brucei* reveals a trypanosome-specific pattern of rRNA modification. *Rna*, **11**, 619–645.

45. Rajan,K.S., Chikne,V., Decker,K., Waldman Ben-Asher,H. and Michaeli,S. (2019) Unique aspects of rRNA biogenesis in trypanosomatids. *Trends Parasitol.*, **35**, 778–794.

46. Chikne,V., Rajan,K.S., Shalev-Benami,M., Decker,K., Cohen-Chalamish,S., Madmoni,H., Biswas,V.K., Gupta,S.K., Doniger,T., Unger,R. *et al.* (2019) Small nucleolar RNAs controlling rRNA processing in *Trypanosoma brucei*. *Nucleic Acids Res.*, **47**, 2609–2629.

47. Tomecki,R., Sikorski,P.J. and Zakrzewska-Placzek,M. (2017) Comparison of preribosomal RNA processing pathways in yeast, plant and human cells – focus on coordinated action of endo- and exoribonucleases. *FEBS Lett.*, **591**, 1801–1850.

48. Bohnsack,K.E. and Bohnsack,M.T. (2019) Uncovering the assembly pathway of human ribosomes and its emerging links to disease. *EMBO J.*, **38**, e100278.

49. Schmid,M. and Jensen,T.H. (2008) The exosome: a multipurpose RNA-decay machine. *Trends Biochem. Sci.*, **33**, 501–510.

50. Lebreton,A., Tomecki,R., Dziembowski,A. and Séraphin,B. (2008) Endonucleolytic RNA cleavage by a eukaryotic exosome. *Nature*, **456**, 993–996.

51. Lorentzen,E., Basquin,J., Tomecki,R., Dziembowski,A. and Conti,E. (2008) Structure of the active subunit of the yeast exosome core, Rrp44: diverse modes of substrate recruitment in the RNase II nuclease family. *Mol. Cell*, **29**, 717–728.

52. Schaeffer,D., Reis,F.P., Johnson,S.J., Arraiano,C.M. and Van Hoof,A. (2012) The CR3 motif of Rrp44p is important for interaction with the core exosome and exosome function. *Nucleic Acids Res.*, **40**, 9298–9307.

53. Schneider,C., Leung,E., Brown,J. and Tollervey,D. (2009) The N-terminal PIN domain of the exosome subunit Rrp44 harbors endonuclease activity and tethers Rrp44 to the yeast core exosome. *Nucleic Acids Res.*, **37**, 1127–1140.

54. Dziembowski,A., Lorentzen,E., Conti,E. and Séraphin,B. (2007) A single subunit, Dis3, is essentially responsible for yeast exosome core activity. *Nat. Struct. Mol. Biol.*, **14**, 15–22.

55. Schneider,C., Anderson,J.T. and Tollervey,D. (2007) The exosome subunit Rrp44 plays a direct role in RNA substrate recognition. *Mol. Cell*, **27**, 324–331.

56. Tomecki,R., Kristiansen,M.S., Lykke-Andersen,S., Chlebowski,A., Larsen,K.M., Szczesny,R.J., Drazkowska,K., Pastula,A., Andersen,J.S., Stepien,P.P. *et al.* (2010) The human core exosome interacts with differentially localized processive RNases: HDIS3 and hDIS3L. *EMBO J.*, **29**, 2342–2357.

57. Kobyłecki,K., Drążkowska,K., Kuliński,T.M., Dziembowski,A. and Tomecki,R. (2018) Elimination of 01/A′-A0 pre-rRNA processing by-product in human cells involves cooperative action of two nuclear exosome-associated nucleases: RRP6 and Dis3. *RNA*, **24**, 1677–1692.

58. Estévez,A.M., Kempf,T. and Clayton,C. (2001) The exosome of *Trypanosoma brucei*. *EMBO J.*, **20**, 3831–3839.

59. Estévez,A.M., Lehner,B., Sanderson,C.M., Ruppert,T. and Clayton,C. (2003) The roles of intersubunit interactions in exosome stability. *J. Biol. Chem.*, **278**, 34943–34951.

60. Cristodero,M., Böttcher,B., Diepholz,M., Scheffzek,K. and Clayton,C. (2008) The *Leishmania tarentolae* exosome: purification and structural analysis by electron microscopy. *Mol. Biochem. Parasitol.*, **159**, 24–29.

61. Makino,D.L., Baumgäerner,M. and Conti,E. (2013) Crystal structure of an RNA-bound 11-subunit eukaryotic exosome complex. *Nature*, **495**, 70–75.

62. Makino,D.L., Schuch,B., Stegmann,E., Baumgärtner,M., Basquin,C. and Conti,E. (2015) RNA degradation paths in a 12-subunit nuclear exosome complex. *Nature*, **524**, 54–58.

63. Zinder,J.C., Wasmuth,E.V and Lima,C.D. (2016) Nuclear RNA exosome at 3.1 Å reveals reveals substrate specificities, RNA paths, and allosteric inhibition of Rrp44/Dis3. *Mol. Cell*, **64**, 734–745.

64. Cesaro,G., Carneiro,F.R.G., Ávila,A.R., Zanchin,N.I.T. and Guimarães,B.G. (2019) *Trypanosoma brucei* RRP44 is involved in an early stage of large ribosomal subunit RNA maturation. *RNA Biol.*, **16**, 133–143.

65. Aphasizheva,I., Ringpis,G.E., Weng,J., Gershon,P.D., Lathrop,R.H. and Aphasizhev,R. (2009) Novel TUTase associates with an editosome-like complex in mitochondria of *Trypanosoma brucei*. *Rna*, **15**, 1322–1337.

66. Shikha,S. and Schneider,A. (2020) The single CCA-adding enzyme of *T. brucei* has distinct functions in the cytosol and in mitochondria. *J. Biol. Chem.*, **295**, 6138–6150.

67. Ericson,M., Janes,M.A., Butter,F., Mann,M., Ullu,E. and Tschudi,C. (2014) On the extent and role of the small proteome in the parasitic eukaryote *Trypanosoma brucei*. *BMC Biol.*, **12**, 14.

68. Carbajo,C.G., Cornell,L.J., Madbouly,Y., Lai,Z., Yates,P.A., Tinti,M. and Tiengwe,C. (2021) Novel aspects of iron homeostasis in pathogenic bloodstream form *Trypanosoma brucei*. *PLoS Pathog.*, **17**, e1009696.

69. Jiang,Y. and Price,D.H. (2004) Rescue of the TTF2 knockdown phenotype with an siRNA-resistant replacement vector. *Cell Cycle*, **3**, 1149–1151.

70. Wirtz,E., Leal,S., Ochatt,C. and Cross,G.A.M. (1999) A tightly regulated inducible expression system for conditional gene knock-outs and dominant-negative genetics in *Trypanosoma brucei*. *Mol. Biochem. Parasitol.*, **99**, 89–101.

71. Wickstead,B., Ersfeld,K. and Gull,K. (2002) Targeting of a tetracycline-inducible expression system to the transcriptionally silent minichromosomes of *Trypanosoma brucei*. *Mol. Biochem. Parasitol.*, **125**, 211–216.

72. Niemirowicz,G.T., Cazzulo,J.J., Álvarez,V.E. and Bouvier,L.A. (2018) Simplified inducible system for *Trypanosoma brucei*. *PLoS One*, **13**, e0205527.

73. Oberholzer,M., Morand,S., Kunz,S. and Seebeck,T. (2006) A vector series for rapid PCR-mediated C-terminal in situ tagging of *Trypanosoma brucei* genes. *Mol. Biochem. Parasitol.*, **145**, 117–120.

74. Brun,R. and Schönenberger (1979) Cultivation and in vitro cloning or procyclic culture forms of *Trypanosoma brucei* in a semi-defined medium. *Acta Trop.*, **36**, 289–292.

75. Pfaffl,M.W. (2001) A new mathematical model for relative quantification in real-time RT-PCR. *Nucleic Acids Res.*, **29**, 16–21.

76. Gradia,D.F., Rau,K., Umaki,A.C.S., de Souza,F.S.P., Probst,C.M., Correa,A., Holetz,F.B., Avila,A.R., Krieger,M.A., Goldenberg,S. *et al.* (2009) Characterization of a novel obg-like ATPase in the protozoan *Trypanosoma cruzi*. *Int. J. Parasitol.*, **39**, 49–58.

77. Church,G.M. and Gilbert,W. (1984) Genomic sequencing. *Proc. Natl. Acad. Sci. U.S.A.*, **81**, 1991–1995.

78. Schneider,C.A., Rasband,W.S. and Eliceiri,K.W. (2012) NIH image to ImageJ: 25 years of image analysis. *Nat. Methods*, **9**, 671–675.

79. Wang,M., Anikin,L. and Pestov,D.G. (2014) Two orthogonal cleavages separate subunit RNAs in mouse ribosome biogenesis. *Nucleic Acids Res.*, **42**, 11180–11191.

80. Medina-Acosta,E. and Cross,G.A.M. (1993) Rapid isolation of DNA from trypanosomatid protozoa using a simple 'mini-prep' procedure. *Mol. Biochem. Parasitol.*, **59**, 327–329.

81. Barth,S., Shalem,B., Hury,A., Tkacz,I.D., Liang,X.H., Uliel,S., Myslyuk,I., Doniger,T., Salmon-Divon,M., Unger,R. *et al.* (2008) Elucidating the role of C/D snoRNA in rRNA processing and modification in *Trypanosoma brucei. Eukaryot. Cell*, **7**, 86–101.

82. Michaeli,S., Doniger,T., Gupta,S.K., Wurtzel,O., Romano,M., Visnovezky,D., Sorek,R., Unger,R. and Ullu,E. (2012) RNA-seq analysis of small RNPs in *Trypanosoma brucei* reveals a rich repertoire of non-coding RNAs. *Nucleic Acids Res.*, **40**, 1282–1298.

83. Kala,S., Mehta,V., Yip,C.W., Moshiri,H., Najafabadi,H.S., Ma,R., Nikpour,N., Zimmer,S.L. and Salavati,R. (2017) The interaction of a *Trypanosoma brucei* KH-domain protein with a ribonuclease is implicated in ribosome processing. *Mol. Biochem. Parasitol.*, **211**, 94–103.

84. Faktorová,D., Bär,A., Hashimi,H., McKenney,K., Horák,A., Schnaufer,A., Rubio,M.A.T., Alfonzo,J.D. and Lukeš,J. (2018) TbUTP10, a protein involved in early stages of pre-18S rRNA processing in *Trypanosoma brucei. Mol. Biochem. Parasitol.*, **225**, 84–93.

85. Hartshorne,T. and Toyofuku,W. (1999) Two 5'-ETS regions implicated in interactions with U3 snoRNA are required for small subunit rRNA maturation in *Trypanosoma brucei. Nucleic Acids Res.*, **27**, 3300–3309.

86. Sakyiama,J., Zimmer,S.L., Ciganda,M., Williams,N. and Read,L.K. (2013) Ribosome biogenesis requires a highly diverged XRN family 5'→3' exoribonuclease for rRNA processing in *Trypanosoma brucei. RNA*, **19**, 1419–1431.

87. Jensen,B.C., Brekken,D.L., Randall,A.C., Kifer,C.T. and Parsons,M. (2005) Species specificity in ribosome biogenesis: a nonconserved phosphoprotein is required for formation of the large ribosomal subunit in *Trypanosoma brucei. Eukaryot. Cell*, **4**, 30–35.

88. Hartshorne,T., Toyofuku,W. and Hollenbaugh,J. (2001) *Trypanosoma brucei* 5'ETS A'-cleavage is directed by 3'-adjacent sequences, but not two U3 snoRNA-binding elements, which are all required for subsequent pre-small subunit rRNA processing events. *J. Mol. Biol.*, **313**, 733–749.

89. Rajan,K.S., Doniger,T., Cohen-Chalamish,S., Rengaraj,P., Galili,B., Aryal,S., Unger,R., Tschudi,C. and Michaeli,S. (2020) Developmentally regulated novel non-coding anti-sense regulators of mRNA translation in *Trypanosoma brucei. Iscience*, **23**, 101780.

90. Zeiner,G.M., Sturm,N.R. and Campbell,D.A. (2003) Exportin 1 mediates nuclear export of the kinetoplastid spliced leader RNA. *Eukaryot. Cell*, **2**, 222–230.

91. Zeiner,G.M., Foldynová,S., Sturm,N.R., Lukeš,J. and Campbell,D.A. (2004) SmD1 Is required for spliced leader RNA biogenesis. *Eukaryot. Cell*, **3**, 241–244.

92. Zeiner,G.M., Hitchcock,R.A., Sturm,N.R. and Campbell,D.A. (2004) 3'-End polishing of the kinetoplastid spliced leader RNA is performed by SNIP, a 3'→5' exonuclease with a motley assortment of small RNA substrates. *Mol. Cell. Biol.*, **24**, 10390–10396.

93. Mandelboim,M., Barth,S., Biton,M., Liang,X.H. and Michaeli,S. (2003) Silencing of Sm proteins in *Trypanosoma brucei* by RNA interference captured a novel cytoplasmic intermediate in spliced leader RNA biogenesis. *J. Biol. Chem.*, **278**, 51469–51478.

94. Foldynová-Trantírková,S., Paris,Z., Sturm,N.R., Campbell,D.A. and Lukeš,J. (2005) The *Trypanosoma brucei* La protein is a candidate poly(U) shield that impacts spliced leader RNA maturation and tRNA intron removal. *Int. J. Parasitol.*, **35**, 359–366.

95. Tomecki,R., Drazkowska,K., Kucinski,I., Stodus,K., Szczesny,R.J., Gruchota,J., Owczarek,E.P., Kalisiak,K. and Dziembowski,A. (2014) Multiple myeloma-associated hDIS3 mutations cause perturbations in cellular RNA metabolism and suggest hDIS3 PIN domain as a potential drug target. *Nucleic Acids Res.*, **42**, 1270–1290.

96. Bonneau,F., Basquin,J., Ebert,J., Lorentzen,E. and Conti,E. (2009) The yeast exosome functions as a macromolecular cage to channel RNA substrates for degradation. *Cell*, **139**, 547–559.

97. Michaeli,S. (2012) rRNA biogenesis in trypanosomes. In: Bindereif,A. (ed). *RNA Metabolism in Trypanosomes*. Springer Berlin Heidelberg, Heidelberg, pp. 123–148.

98. Fleming,I.M.C., Paris,Z., Gaston,K.W., Balakrishnan,R., Fredrick,K., Rubio,M.A.T. and Alfonzo,J.D. (2016) A tRNA methyltransferase paralog is important for ribosome stability and cell division in *Trypanosoma brucei. Sci. Rep.*, **6**, 21438.

99. Allmang,C., Mitchell,P., Petfalski,E. and Tollervey,D. (2000) Degradation of ribosomal RNA precursors by the exosome. *Nucleic Acids Res.*, **28**, 1684–1691.

100. Wery,M., Ruidant,S., Schillewaert,S., Leporé,N. and Lafontaine,D.L.J. (2009) The nuclear poly(A) polymerase and exosome cofactor Trf5 is recruited cotranscriptionally to nucleolar surveillance. *RNA*, **15**, 406–419.

101. Kos-Braun,I.C., Jung,I. and Koš,M. (2017) Tor1 and CK2 kinases control a switch between alternative ribosome biogenesis pathways in a growth-dependent manner. *PLoS Biol.*, **15**, e2000245.

102. Allmang,C., Petfalski,E., Podtelejnikov,A., Mann,M., Tollervey,D. and Mitchell,P. (1999) The yeast exosome and human PM-Scl are related complexes of 3' → 5' exonucleases. *Genes Dev.*, **13**, 2148–2158.

103. Kumakura,N., Otsuki,H., Tsuzuki,M., Takeda,A. and Watanabe,Y. (2013) *Arabidopsis* AtRRP44A is the functional homolog of Rrp44/Dis3, an exosome component, is essential for viability and is required for RNA processing and degradation. *PLoS One*, **8**, e79219.

104. Preti,M., O'Donohue,M.F., Montel-Lehry,N., Bortolin-Cavaillé,M.L., Choesmel,V. and Gleizes,P.E. (2013) Gradual processing of the ITS1 from the nucleolus to the cytoplasm during synthesis of the human 18S rRNA. *Nucleic Acids Res.*, **41**, 4709–4723.

105. Sloan,K.E., Mattijssen,S., Lebaron,S., Tollervey,D., Pruijn,G.J.M. and Watkins,N.J. (2013) Both endonucleolytic and exonucleolytic cleavage mediate ITS1 removal during human ribosomal RNA processing. *J. Cell Biol.*, **200**, 577–588.

106. Sikorski,P.J., Zuber,H., Philippe,L., Sement,F.M., Canaday,J., Kufel,J., Gagliardi,D. and Lange,H. (2015) Distinct 18S rRNA precursors are targets of the exosome complex, the exoribonuclease RRP6L2 and the terminal nucleotidyltransferase TRL in *Arabidopsis thaliana. Plant J.*, **2**, 991–1004.

107. Umaer,K., Ciganda,M. and Williams,N. (2014) Ribosome biogenesis in African trypanosomes requires conserved and trypanosome-specific factors. *Eukaryot. Cell*, **13**, 727–737.

108. Jensen,B.C., Wang,Q., Kifer,C.T. and Parsons,M. (2003) The NOG1 GTP-binding protein is required for biogenesis of the 60 S ribosomal subunit. *J. Biol. Chem.*, **278**, 32204–32211.

109. Gupta,S.K., Chikne,V., Eliaz,D., Tkacz,I.D., Naboishchikov,I., Carmi,S., Ben-Asher,H.W. and Michaeli,S. (2014) Two splicing factors carrying serine-arginine motifs, TSR1 and TSR1IP, regulate splicing, mRNA stability, and rRNA processing in *Trypanosoma brucei. RNA Biol.*, **11**, 715–731.